iScience

CellPress
OPEN ACCESS

Article

# YTHDF2-mediated circYAP1 drives immune escape and cancer progression through activating YAP1/TCF4-PD-L1 axis

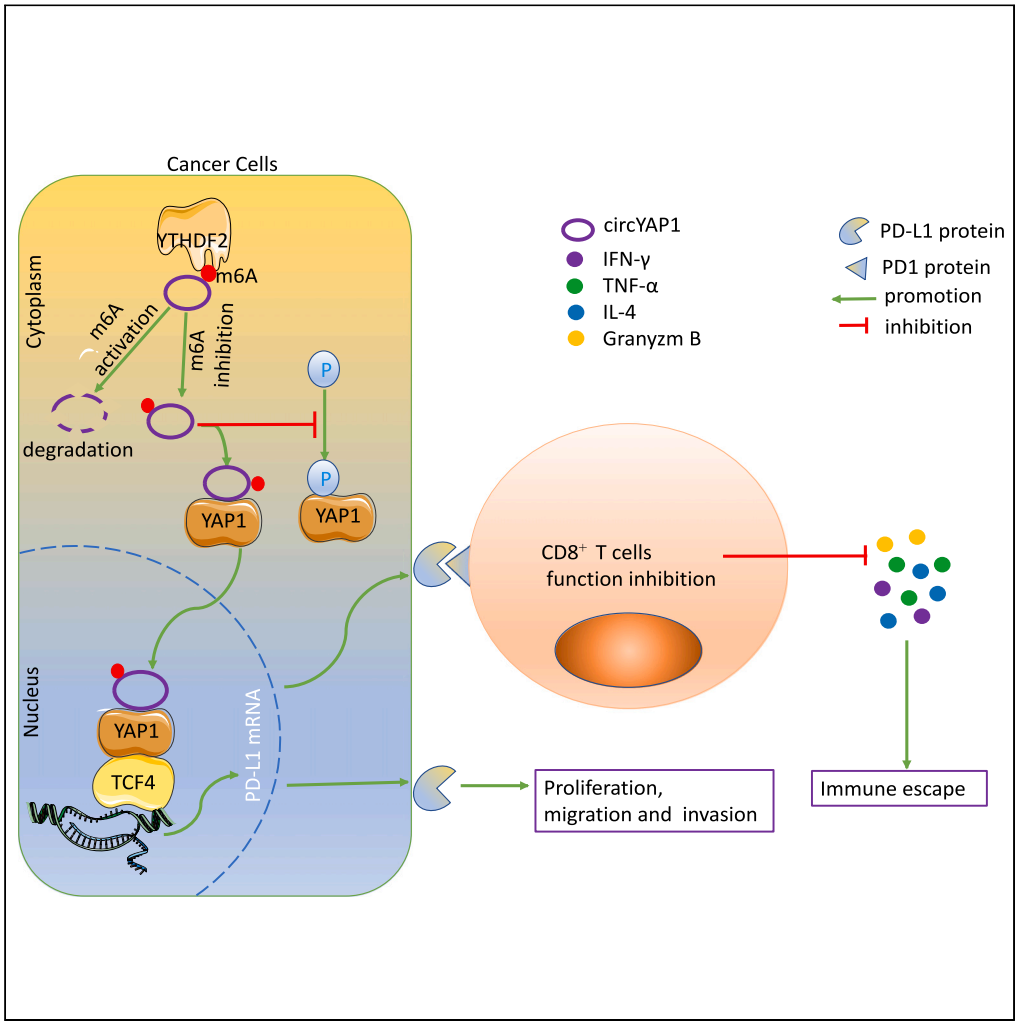


Zhuang Chen, Wenkang Wang, Shengyun Hu, ..., Chengzeng Wang, Yang Liu, Zhenqiang Sun

czw202112@zzu.edu.cn (C.W.)
zlyyliuyang1440@zzu.edu.cn (Y.L.)
fccsunzq@zzu.edu.cn (Z.S.)

## Highlights

CircYAP1 affects prognosis of CRC patients

CircYAP1 promotes CRC immune escape

CircYAP1 bounds YAP1 protein to promote the PD-L1 promoter transcription in CRC cells

YTHDF2 degrades circYAP1

Chen et al., iScience *27*, 108779
February 16, 2024 
https://doi.org/10.1016/j.isci.2023.108779

iScience

CellPress
OPEN ACCESS

Article

# YTHDF2-mediated circYAP1 drives immune escape and cancer progression through activating YAP1/TCF4-PD-L1 axis

Zhuang Chen,[1,2,8] Wenkang Wang,[3,8] Shengyun Hu,[1] Haifeng Sun,[1] Chen Chen,[2] Zhiyong Zhang,[1] Xinzhi Sun,[4] Bin Jia,[5] Junhong Hu,[1] Chengzeng Wang,[2,6,*] Yang Liu,[7,*] and Zhenqiang Sun[1,2,9,*]

## SUMMARY

**Immune escape is identified as one of the reasons for the poor prognosis of colorectal cancer (CRC) patients. Circular RNAs are considered to promote tumor progression by mediating tumor immune escape. We discovered that higher expression of circYAP1 was associated with a worse prognosis of CRC patients. Functional experiments *in vitro* and *in vivo* showed that circYAP1 upregulation inhibited the cytotoxicity of $CD8^+$ T cells by upregulating programmed death ligand-1 (PD-L1). Mechanistically, we found that circYAP1 directly binds to the YAP1 protein to prevent its phosphorylation, enhancing proportion of YAP1 protein in the nucleus, and that YAP1 interacts with TCF4 to target the PD-L1 promoter and initiate PD-L1 transcription in CRC cells. Taken together, circYAP1 promotes CRC immune escape and tumor progression by activating the YAP1/TCF4-PD-L1 axis and may provide a new strategy for combination immunotherapy of CRC patients.**

## INTRODUCTION

Colorectal cancer (CRC) is one of the most common malignancies of the gastrointestinal system. Globally, CRC has the third highest incidence rate, and the mortality rate is only exceeded by lung cancer, with a continuously increasing trend in recent years.[1–3] In recent years, immunotherapies have been proven to prevent tumor progression and provide long-term clinical benefits in patients with malignancies.[4] However, most patients with solid tumors are not always sensitive to immunotherapy drugs,[5] so the molecular mechanisms that regulate tumor immune escape need to be further explored.

An essential part of the tumor immune escape mechanism is that programmed death ligand-1 (PD-L1) binds programmed death-1 (PD1) to protect cancer cells from cytotoxic T lymphocyte killing.[6] $CD8^+$ T cells secrete γ-interferon (IFN-γ),[7] tumor necrosis factor alpha (TNF-α),[8] interleukin-4 (IL-4),[9] and Granyzm B[10] to kill cancer cells. PD-L1/PD1 inhibits cytokine secretion by $CD8^+$ T cells. PD-L1 on cancer cells is regulated by a variety of factors in tumors: posttranslational modifications of the PD-L1 protein (ubiquitination modifications,[11] acetylations,[12] etc.) and protein localization (being secreted into the extracellular microenvironment and being translocated to the nucleus[13]) play powerful roles in regulating the immunotherapeutic response. In addition, PD-L1 is regulated by transcription factors in tumor tissues. For example, Yes-associated protein 1 (YAP1) interacts with other transcription factors to enhance the transcriptional activity of the PD-L1 promoter to upregulate PD-L1 expression in cancer cells.[14–16] It is known that circular RNAs (circRNAs) modify PD-L1 mRNA expression by sponging microRNAs (miRNAs),[17] but it remains unclear whether circRNAs promote PD-L1 transcription in an RNA-binding protein (RBP) manner.

In this study, we first explored the potential of circYAP1 as a prognostic biomarker. Then, we identified its role in promoting colon cancer cell immune evasion by activating the YAP1/TCF4-PD-L1 axis. Our further analysis revealed that m6A exists on circYAP1. The m6A reader protein YTHDF2 could accelerate m6A-circYAP1 degradation in colon cancer cells. These results may provide a new therapeutic target for controlling CRC immune escape.

[1]Department of Colorectal Surgery, The First Affiliated Hospital of Zhengzhou University, Zhengzhou, Henan 450052, China
[2]Henan Institute of Interconnected Intelligent Health Management, The First Affiliated Hospital of Zhengzhou University, Zhengzhou, Henan 450052, China
[3]Department of Breast Surgery, The First Affiliated Hospital of Zhengzhou University, Zhengzhou, Henan 450052, China
[4]Department of Orthopaedics, The First Affiliated Hospital of Zhengzhou University, Zhengzhou, Henan 450052, China
[5]Department of Oncology, the First Affiliated Hospital of Zhengzhou University, Zhengzhou, Henan 450052, China
[6]Department of Ultrasound, The First Affiliated Hospital of Zhengzhou University, Zhengzhou, Henan 450052, China
[7]Department of Radiotherapy, The Affiliated Cancer Hospital of Zhengzhou University & Henan Cancer Hospital, Zhengzhou 450008, China
[8]These authors contributed equally
[9]Lead contact
*Correspondence: czw202112@zzu.edu.cn (C.W.), zlyyliuyang1440@zzu.edu.cn (Y.L.), fccsunzq@zzu.edu.cn (Z.S.)
https://doi.org/10.1016/j.isci.2023.108779

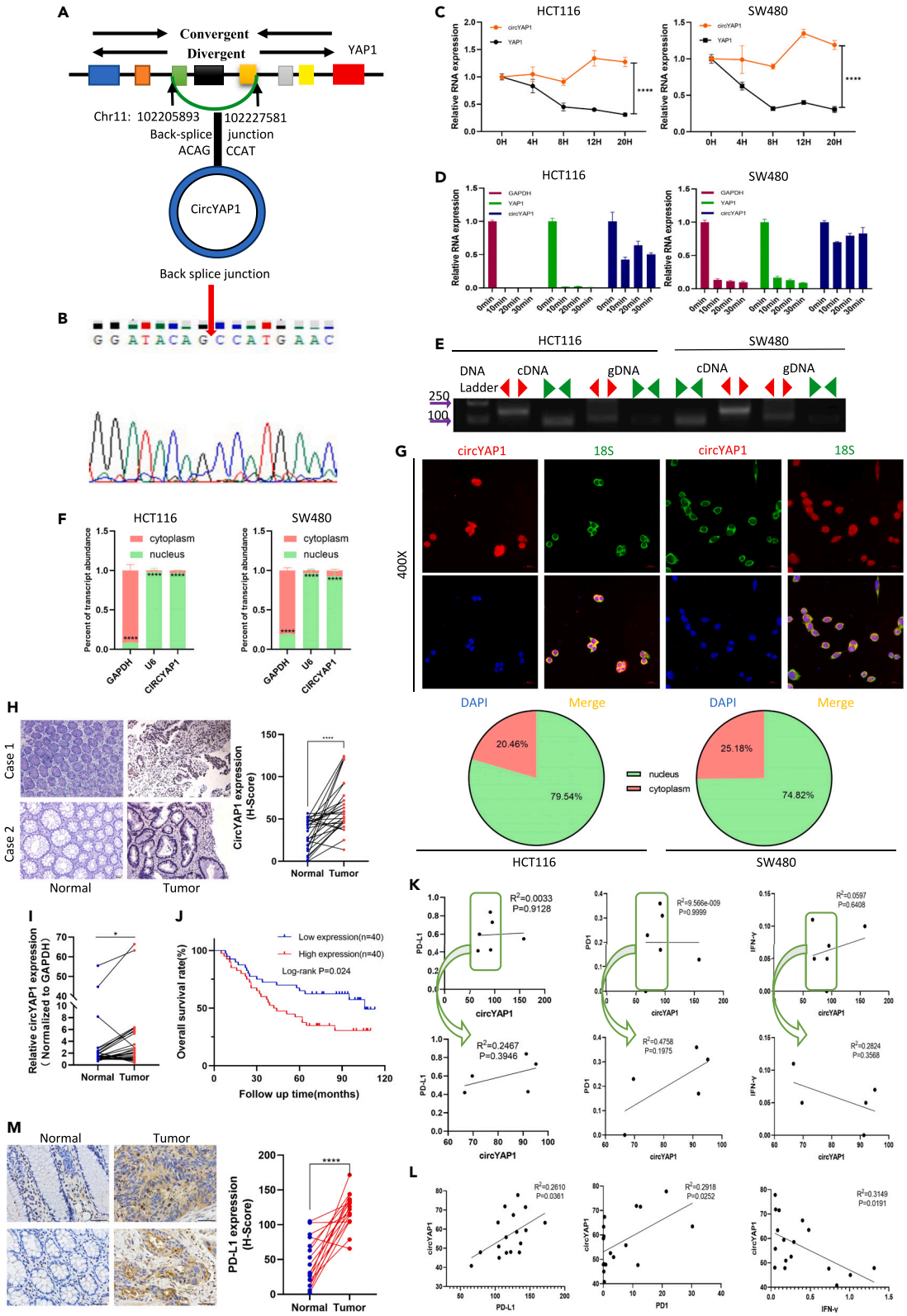
A
Convergent
Divergent
YAP1
Chr11: 102205893
Back-splice
ACAG
102227581
junction
CCAT
CircYAP1
Back splice junction
B
G G A T A C A G C C A T G A A C
C
HCT116
SW480
circYAP1
YAP1
Relative RNA expression
0H 4H 8H 12H 20H
D
HCT116
SW480
GAPDH
YAP1
circYAP1
Relative RNA expression
0min 10min 20min 30min
E
HCT116
SW480
DNA Ladder
cDNA
gDNA
250
100
F
HCT116
SW480
cytoplasm
nucleus
Percent of transcript abundance
GAPDH
U6
CIRCYAP1
G
circYAP1
18S
400X
DAPI
Merge
20.46%
79.54%
25.18%
74.82%
nucleus
cytoplasm
H
Case 1
Case 2
Normal
Tumor
CircYAP1 expression (H-Score)
I
Relative circYAP1 expression ( Normalized to GAPDH)
J
Low expression(n=40)
High expression(n=40)
Log-rank P=0.024
Overall survival rate(%)
Follow up time(months)
K
PD-L1
PD1
IFN-γ
circYAP1
R²=0.0033
P=0.9128
R²=9.566e-009
P=0.9999
R²=0.0597
P=0.6408
R²=0.2467
P=0.3946
R²=0.4758
P=0.1975
R²=0.2824
P=0.3568
L
R²=0.2610
P=0.0361
R²=0.2918
P=0.0252
R²=0.3149
P=0.0191
M
Normal
Tumor
PD-L1 expression (H-Score)

**Figure 1. CircYAP1 was highly expressed in CRC tissues and positively correlated with PD-L1**

(A) The process of circYAP1 formation and its location in the human genome.

(B) The result of Sanger sequence for circYAP1 using a divergent primer.

(C) The abundance of circYAP1 and YAP1 mRNA in HCT116 and SW480 cells cultured with actinomycin D at 0, 4, 8, 12, and 20 h were analyzed by RT-qPCR (n = 4 each group was made in quadruplicate, unpaired t test).

(D) The expressions of circYAP1 and YAP1 mRNA after Rnase R treatment were analyzed by RT-qPCR.

(E) Verification of the loop structure of circYAP1 through convergent and divergent primers.

(F) Analysis of the expression levels of circYAP1 in the cytoplasm and nucleus by RT-qPCR in HCT116 and SW480 cells (n = 4 each group was made in quadruplicate, unpaired t test).

(G) FISH was performed to observe the cellular location of circYAP1 (red) and 18S (green) in cells (Scale bar: 20 μm).

(H) Typical ISH images and ISH scores analysis of circYAP1 in CRC tissues and normal tissues (Scale bar: 50 μm n = 28 pairs of tissues, paired t test).

(I) circYAP1 expression in 28 pairs of CRC tissues and normal tissues detected by RT-qPCR (n = 28 pairs of tissues, paired t test).

(J) The overall survival analysis of circYAP1 from 80 CRC patients (Kaplan-Meier's method and log rank tests, n = 40 patients with circYAP1 low expression and n = 40 patients with circYAP1 high expression).

(K) Correlation analysis of circYAP1 with PD-L1, PD1, and IFN-γ in high-throughput sequencing data (Spearman correlation coefficient analyses, n = 6 CRC tissues in top and n = 5 CRC tissues in down).

(L) Correlation analysis of circYAP1 with PD-L1, PD1, and IFN-γ in 17 CRC tissues (Spearman correlation coefficient analyses, n = 17 CRC tissues).

(M) Typical IHC images and IHC scores analysis of PD-L1 in 17 CRC tissues and normal tissues (Scale bar: 50 μm n = 17 pairs of tissues, paired t test). Data are shown as means ± SD, *p < 0.05, ****p < 0.0001.

## RESULTS

### CircYAP1 was highly expressed in CRC tissues and positively correlated with PD-L1

We reported that circ1662, circ1663 (circYAP1), circ7809, and circ4958, derived from YAP1, were highly expressed in CRC tissues compared to paracancerous tissues in our previous study.[18] Here, we explored the functional mechanism of circYAP1 in more detail. CircYAP1 consists of backsplicing of 3 exons of the YAP1 gene and has a length of 426 bp (Figure 1A). The backsplice site of circYAP1 was verified by Sanger sequencing (Figure 1B). CircYAP1 was characterized as more stable than YAP1 mRNA in actinomycin D-treated HCT116 and SW480 cells (Figure 1C) and was resistant to RNase R digestion (Figure 1D). Additionally, circYAP1 could be amplified by divergent primers from complementary DNA (cDNA) rather than genomic DNA (gDNA) of HCT116 and SW480 cells (Figure 1E). Consistent with quantitative reverse-transcription PCR (RT-qPCR) of nuclear and cytoplasmic fractions, fluorescence *in situ* hybridization (FISH) also showed that circYAP1 was observed in both the cytoplasm and nucleus, but mainly in the nucleus (Figures 1F and 1G). These results verified the loop structure of circYAP1.

To further investigate the expression of circYAP1 in CRC, we performed *in situ* hybridization (ISH) on 28 paired CRC tissues from our hospital. The ISH results demonstrated that circYAP1 was expressed at significantly higher levels in CRC tissues than in normal tissues (Figure 1H). In addition, we performed RT-qPCR to analyze circYAP1 expression in each pair of patient samples. A higher expression level of circYAP1 was identified in cancer tissues than in normal tissues (Figure 1I). Next, we verified the negative clinical significance of circYAP1 in CRC patients. We detected circYAP1 levels in 80 CRC tissues by RT-qPCR. We found that higher circYAP1 expression was associated with lymph node metastasis and later clinical stage (Table 1). Survival analysis showed that high circYAP1 expression predicted shorter overall survival of CRC patients (Figure 1J).

Further analysis of the sequencing data revealed that circYAP1 showed a positive association with PD1/PD-L1 and a negative association with IFN-γ in five CRC patients, although the p value was greater than 0.05 (Figure 1K). Considering that the small sample sizes did not yield any statistically significant results, we performed immunohistochemistry (IHC) for PD-L1, PD1, and IFN-γ in a larger number of CRC tissues. The results confirmed that circYAP1 was positively associated with PD1/PD-L1 and negatively associated with IFN-γ in CRC patients (Figure 1L). Meanwhile, the results showed that PD-L1 had higher expression in CRC tissues than in normal tissues (Figure 1M). Based on this evidence, we speculate that circYAP1 may upregulate PD-L1 expression in cancer cells to suppress the immune function of $CD8^+$ T cells. This implies that circYAP1 may function as an oncogenic factor and is likely to be involved in immune escape.

### CircYAP1 significantly promoted tumor immune escape and affected CRC cell proliferation, migration, and invasion *in vitro*

PD-L1 on tumor cells mediates immune escape by inhibiting the cytotoxic effects of $CD8^+$ T cells by binding to PD1 on $CD8^+$ T cells.[19] To investigate the potential contribution of circYAP1 to immune escape, we constructed a circYAP1 overexpression plasmid. RT-qPCR analysis confirmed that circYAP1 expression was elevated in HCT116 and SW480 cells that were transfected with the circYAP1 overexpression plasmid (Figure 2A). Then, we isolated $CD8^+$ T cells from the peripheral blood of healthy volunteers to coculture tumor cells. After coincubation for 48 h, cytokines (IFN-γ, TNF-α, IL-4, and Granyzm B) in $CD8^+$ T cells were measured by RT-qPCR. It was evident that IFN-γ, TNF-α, IL-4, and Granyzm B in $CD8^+$ T cells cocultured with high circYAP1 tumor cells were inhibited compared to those in negative control (NC) group (Figure 2B). Next, we performed IHC for CD8 on paraffin-embedded CRC tissues. We found that the level of infiltrating $CD8^+$ T cells in low-circYAP1-CRC tissues was higher than the level of those in high-circYAP1-CRC tissues. That is, the $CD8^+$ T cell positive density was negatively correlated with circYAP1 expression (Figures 2C and 2F). Interestingly, the correlation analysis between PD-L1 and CD8 based on IHC and xCELL analysis performed on GSE106584 and GSE87211 data showed that $CD8^+$ T cell infiltration was negatively correlated with PD-L1 expression in CRC patients (Figures 2D–2F). The aforementioned results implied that circYAP1 was involved in the $CD8^+$ T cell exhaustion and functional suppression through the regulation of PD-L1 on tumor cells, ultimately leading to tumor immune escape.

**Table 1. Correlation for clinicopathologic parameters about cirYAP1 level in CRC patients**

| | | circYAP1 expression | | |
|---|---|---|---|---|
| Parameters | Number of cases | High | Low | p value |
| All cases | 80 | | | |
| Gender | | | | 0.496 |
| Male | 47 | 25 | 22 | |
| Female | 33 | 15 | 18 | |
| Age | | | | 0.104 |
| =<60 | 29 | 11 | 18 | |
| >60 | 51 | 29 | 22 | |
| Histological grade | | | | 0.468 |
| I-II | 60 | 31 | 29 | |
| III-IV | 19 | 8 | 11 | |
| Lymph node metastasis | | | | 0.005 |
| No | 41 | 15 | 26 | |
| Yes | 35 | 24 | 11 | |
| Tumor depth | | | | 0.571 |
| T2 | 4 | 1 | 3 | |
| T3 | 17 | 9 | 8 | |
| T4 | 54 | 28 | 26 | |
| Clinical stage | | | | 0.039 |
| I | 4 | 1 | 3 | |
| II | 37 | 14 | 23 | |
| III | 34 | 23 | 11 | |
| IV | 1 | 1 | 0 | |

To gain a more adequate understanding of the function of circYAP1 in CRC, we constructed two additional small interfering RNAs (siRNAs) targeting circYAP1. RT-qPCR analysis confirmed that circYAP1 expression was decreased in siRNA-transfected HCT116 and SW480 cells (Figure S1A). CCK8, EdU, and Transwell assays showed that circYAP1-overexpressing tumor cells exhibited higher proliferation, migration, and invasion capacity, while circYAP1 silencing dramatically inhibited HCT116 and SW480 cell proliferation, migration, and invasion capacity (Figures S2B–S2F). Simultaneously, upregulation of circYAP1 evidently resulted in higher expression of N-cadherin protein and lower expression of E-cadherin protein, and downregulation of circYAP1 evidently resulted in lower expression of N-cadherin protein and higher expression of E-cadherin protein (Figure 3B). These results suggested that circYAP1 enhanced tumor cell proliferation, migration, invasion, and epithelial-mesenchymal transition.

## The oncogenic effect of circYAP1 is dependent on PD-L1

The aforementioned data suggest that circYAP1 might regulate PD-L1 levels in CRC cells. To verify this assumption, we determined whether PD-L1 was changed in circYAP1-upregulated and circYAP1-downregulated HCT116 and SW480 cells. We observed that PD-L1 was reduced with circYAP1 knockdown and elevated with circYAP1 overexpression at both the mRNA and protein levels in HCT116 and SW480 cells (Figures 3A and 3B).

Next, we designed a rescue experiment to explore whether circYAP1 is dependent on PD-L1 to promote immune evasion. RT-qPCR showed that PD-L1 mRNA expression was enhanced by the circYAP1 overexpression plasmid, which was subsequently inhibited by PD-L1 siRNA (Figure S3A). Surprisingly, RT-qPCR showed that lower IFN-γ, TNF-α, IL-4, and Granyzm B levels were produced by $CD8^+$ T cells cocultured with SW480 cells with higher circYAP1 expression. After knockdown of PD-L1 in the circYAP1-overexpressing SW480 cells, cocultured $CD8^+$ T cells expressed higher levels of IFN-γ, TNF-α, IL-4, and Granyzm B (Figure 3C). The GSE19750 analysis results showed that high PD-L1 expression represented worse overall survival (Figure 3D). Interestingly, we found that patients with high PD-L1 expression responded well to anti-PD-L1, while CRC patients with low PD-L1 expression did not respond to anti-PD-L1 in the Wolf cohort 2021 Anti-PD-L1 (Figure 3E). Moreover, for CRC patients treated with immune checkpoint inhibitors, high levels of PD-L1 expression predicted longer overall survival in the Cho cohort 2020 Anti-PD1/PD-L1(Figure 3F).

The nonimmune checkpoint role of PD-L1 has recently been reported.[20] To explore the intrinsic effects of PD-L1 in CRC, we downregulated PD-L1 expression in HCT116 and SW480 cells with siRNA (Figure S4A). CCK8, EdU, and Transwell assays indicated that PD-L1 downregulation hampered the proliferation, migration, and invasion abilities compared to the small interfering RNA-negative control (si-NC) group

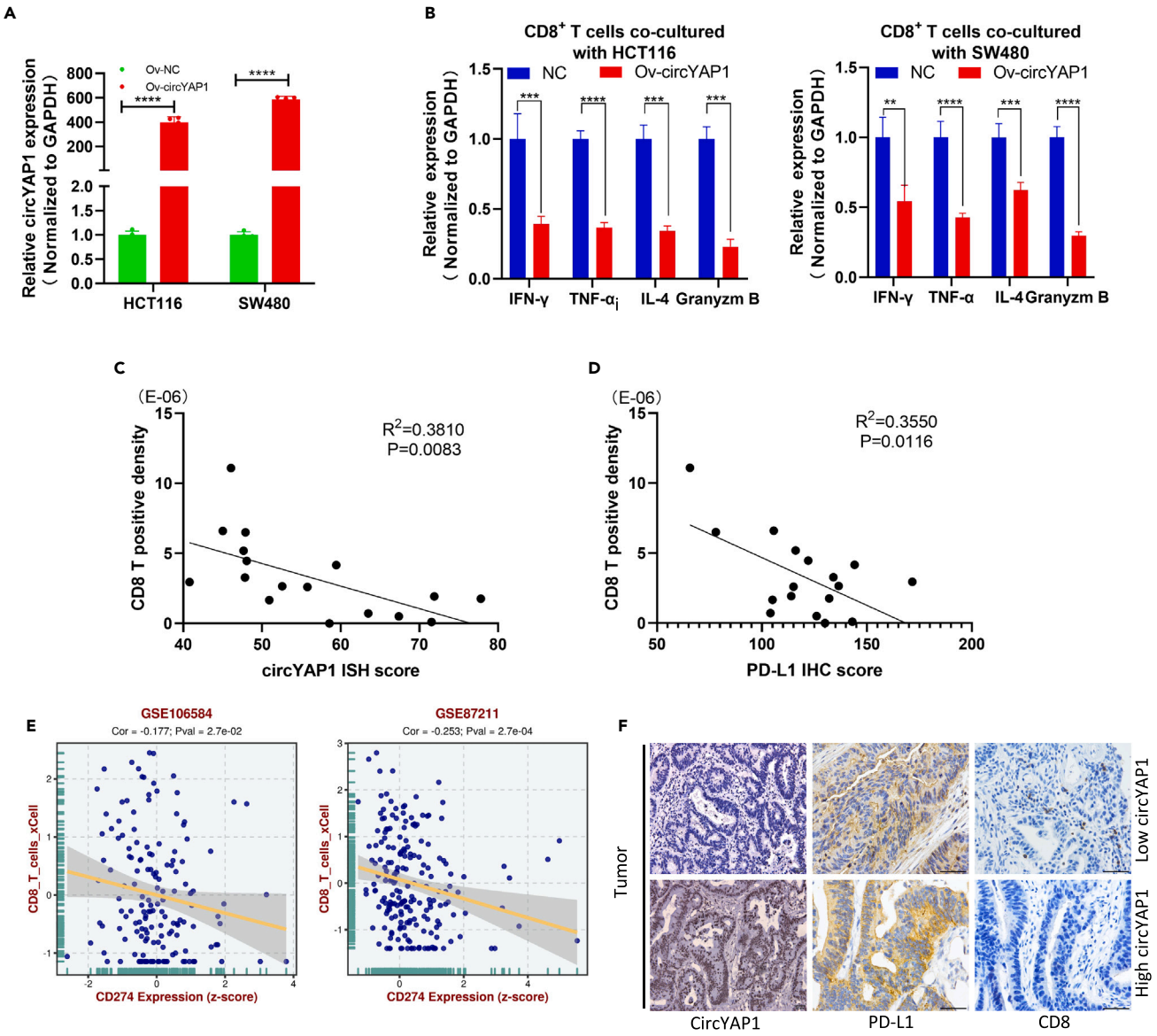


**Figure 2. Effects of circYAP1 on CRC cells immune evasion *in vitro***

(A) RT-qPCR analysis of ov-circYAP1 efficiency in HCT116 and SW480 cells treated with ov-circYAP1 plasmids (n = 4 each group was made in quadruplicate, unpaired t test).

(B) RT-qPCR analysis of IFN-γ, TNF-α, IL-4, and Granyzm B in $CD8^+$ T cells cocultured with circYAP1-overexpressed HCT116 and SW480 cells (n = 4 each group was made in quadruplicate, unpaired t test).

(C and D) Correlation analysis between $CD8^+$ T cells positive density and circYAP1(C) or PD-L1(CD274) (D) in 17 CRC tissues (Spearman correlation coefficient analyses, n = 17 CRC tissues).

(E) Correlation analysis between $CD8^+$ T cells positive density and PD-L1(CD274) in GSE106584 and GSE87211 using BEST application (https://rookieutopia.com/)

(F) Typical IHC images for PD-L1 and CD8 in low/high circYAP1 expressed CRC tissues (Scale bar: 50 μm). Data are expressed as mean ± standard deviation, $^{**}p < 0.01$, $^{***}p < 0.001$, $^{****}p < 0.0001$.

(Figures S4B–S4D). In addition, si-PD-L1 was sufficient to counteract the proliferation-, migration-, and invasion-promoting influence of over-expression (ov)-circYAP1 in HCT116 and SW480 cells (Figures S2A–S2D). These data suggest that circYAP1 regulates PD-L1 to play an immune or nonimmune role in promoting CRC progression.

## CircYAP1 prevents YAP1 protein phosphorylation to drive PD-L1 upregulation

Given that we have found in previous work that circ1662 binds directly to the YAP1 protein, we hypothesize that circYAP1 shares similar characteristics.[18] First, we performed colocalization experiments of circYAP1 and YAP1 proteins by FISH-immunofluorescence (IF). Evidently,

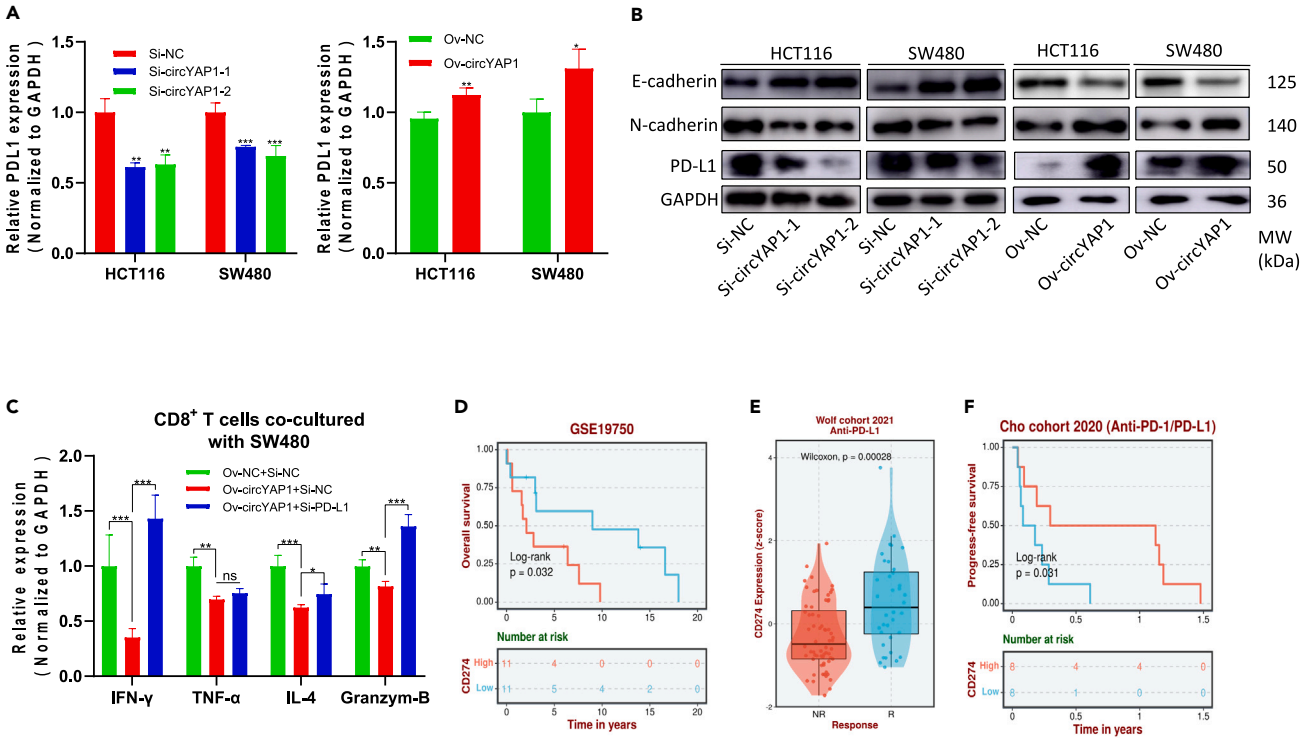


**Figure 3. The immune evasion effect of circYAP1 is dependent on PD-L1**

(A) mRNA expression levels of PD-L1 were determined in HCT116 and SW480 cells after transfected with circYAP1 siRNA and circYAP1 overexpressed plasmids by RT-qPCR (n = 4 each group was made in quadruplicate, ANOVA test in right and unpaired t test in left).

(B) Protein levels of PD-L1, E-cadherin, and N-cadherin were determined in HCT116 and SW480 cells after transfected with circYAP1 siRNA and circYAP1 overexpressed plasmids by western blot (C) RT-qPCR analysis of IFN-γ, TNF-α, IL-4, and Granyzm B in $CD8^+$ T cells cocultured with circYAP1-overexpressed and si-PD-L1 SW480 cells (n = 4 each group was made in quadruplicate, ANOVA test).

(D) The analysis of CRC patients OS of PD-L1 using the data of GSE39582 by BEST application (https://rookieutopia.com/).

(E) The correlation analysis between anti-PD-L1 treatment response and PD-L1 level by BEST application (https://rookieutopia.com/).

(F) The OS of PD-L1 in CRC patient treated with anti-PD1/PD-L1 by BEST application (https://rookieutopia.com/). Data are expressed as mean ± standard deviation, ns $p \geq 0.05$, *$p < 0.05$, **$p < 0.01$, ***$p < 0.001$.

circYAP1 and YAP1 proteins have highly overlapping positional distributions in HCT116 and SW480 cells (Figure 4A). Second, RNA immunoprecipitation (RIP)-qPCR was used to investigate the interaction between circYAP1 and the YAP1 protein. As expected, the YAP1 antibody pulled down the circYAP1 in HCT116 and SW480 cells (Figure 4B). Finally, a biotin-based RNA pull-down assay was performed to validate the target of circYAP1. The CircYAP1 probe was enriched for the YAP1 protein but not the GAPDH protein, while the negative control probe was not enriched for either protein in HCT116 and SW480 cells (Figure 4C). These data demonstrate that circYAP1 directly binds the YAP1 protein.

The p-YAP1 protein has been reported to be mainly distributed in the cytoplasm. Dephosphorylated YAP1 is the only active form that enters the nucleus to stimulate downstream gene transcription.[21] We hypothesized that circYAP1 competitively binds to the YAP1-Ser127 phosphorylation site to increase the proportion of YAP1 protein in the nucleus. Nucleoplasmic separation assays of proteins and IF experiments in HCT116 and SW480 cells were performed. Compared to HCT116 and SW480 cells transfected with a negative control plasmid, the proportion of YAP1 protein was increased in the nucleus of cells transfected with a circYAP1 overexpression plasmid (Figure 4D). At the same time, the proportion of p(ser127)-YAP1 protein was decreased in the cytoplasm (Figures 4D and 4E). Furthermore, we found that YAP1 mutated at the Ser 127 site was no longer able to enrich circYAP1(Figure 4F). These data show that circYAP1 binds to and prevents the phosphorylation sites (Ser 127) of YAP1 increasing the proportion of YAP1 protein in the nucleus.

We then determined whether circYAP1 regulates PD-L1 in CRC cells in a YAP1-dependent manner. The efficiency of the rescue experiment is shown in Figure S3B RT-qPCR and western blot results showed that YAP1 siRNA can reverse the positive regulation of PD-L1 mRNA and protein by circYAP1 overexpression plasmids in HCT116 and SW480 cells (Figures 4G and 4H). Furthermore, circYAP1 overexpression promoted the proliferation, migration, and invasion of HCT116 and SW480 cells, which were impaired by si-YAP1 (Figures 4I–4l). In addition, circYAP1 overexpression reduced E-cadherin and increased N-cadherin expression, and this effect was reversed by si-YAP1 in HCT116 and SW480 cells (Figure 4G).

Taken together, these data imply that circYAP1 regulates PD-L1 expression and nonimmune checkpoint action by enhancing the proportion of YAP1 protein in the nucleus.

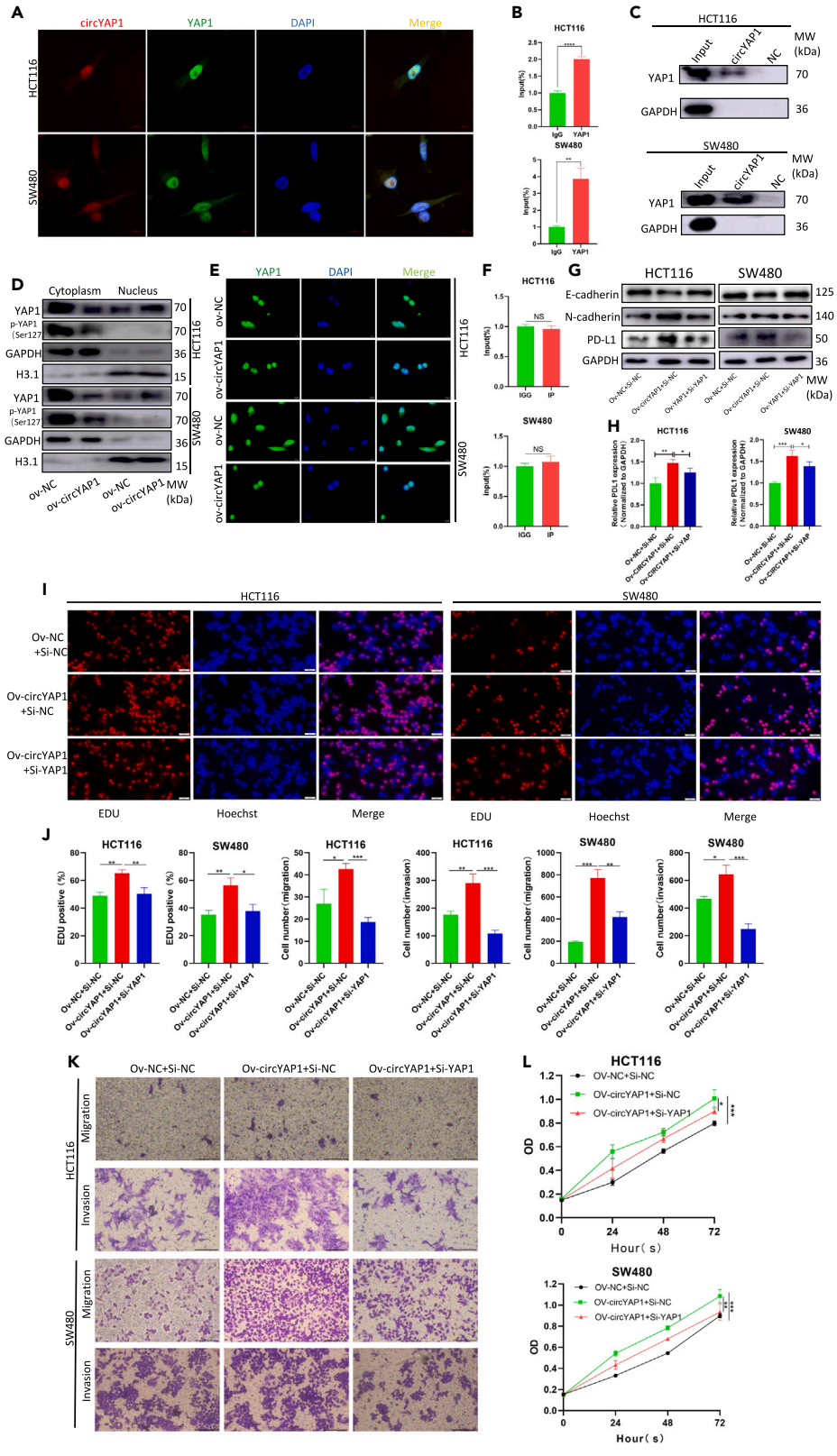
A
circYAP1
YAP1
DAPI
Merge
HCT116
SW480
B
HCT116
Input(%)
IgG
YAP1
SW480
C
HCT116
Input
circYAP1
NC
MW (kDa)
YAP1
GAPDH
70
36
SW480
D
Cytoplasm
Nucleus
YAP1
p-YAP1 (Ser127)
GAPDH
H3.1
70
36
15
ov-NC
ov-circYAP1
MW (kDa)
E
YAP1
DAPI
Merge
F
HCT116
SW480
NS
IGG
IP
G
HCT116
SW480
E-cadherin
N-cadherin
PD-L1
GAPDH
125
140
50
36
Ov-NC+Si-NC
Ov-circYAP1+Si-NC
Ov-YAP1+Si-YAP1
Ov-circYAP1+Si-YAP1
H
Relative PDL1 expression (Normalized to GAPDH)
I
Ov-NC +Si-NC
Ov-circYAP1 +Si-NC
Ov-circYAP1 +Si-YAP1
EDU
Hoechst
Merge
J
EDU positive (%)
Cell number (migration)
Cell number (invasion)
K
Ov-NC+Si-NC
Ov-circYAP1+Si-NC
Ov-circYAP1+Si-YAP1
Migration
Invasion
L
OD
Hour(s)

**Figure 4. CircYAP1 prevents YAP1 protein phosphorylation to drive PD-L1 upregulation**

(A) FISH-IF assay was performed to detected the colocalization of circYAP1 and YAP1 protein in CRC cells (Scale bar: 10 μm).

(B) YAP1-RIP analysis of the directly binding between circYAP1 and YAP1 protein in CRC cells (n = 4 each group was made in quadruplicate, unpaired t test).

(C) CircRNA pull-down assay was performed by biotin-labeled circYAP1 probes in CRC transfected circYAP1 overexpression plasmids.

(D and E) Western blot and IF assays (Scale bar:10 μm) to verify changes in the proportion of YAP1 and p-YAP1 in the cytoplasm and nucleus of CRC cells after transfection with the circYAP1 overexpression plasmid.

(F) RIP analysis of the circYAP1 and YAP1(Ser 127 mut) protein in CRC cells (n = 4 each group was made in quadruplicate, unpaired t test) (G and H) mRNA expression levels of PD-L1 and protein level of PD-L1, E-cadherin, and N-cadherin were determined in CRC cells after transfected with circYAP1 plasmids and si-YAP1 by RT-qPCR (n = 4 each group was made in quadruplicate, ANOVA test) and western blot.

(I–L) Proliferation, migration, and invasion abilities of HCT116 and SW480 cells were determined after transfection with circYAP1 plasmids and si-YAP1 by EDU (Scale bar: 50 μm, n = 3 each group was made in triplicate, ANOVA test), CCK8(n = 5 each group was made in quintuplicate, ANOVA test), and Transwell assays (Scale bar: 100 μm, n = 3 each group was made in triplicate, ANOVA test). Data are expressed as mean ± standard deviation, *p < 0.05, **p < 0.01, ***p < 0.001, ****p < 0.0001.

## YAP1 combined with TCF4 regulates PD-L1 expression to inhibit CD8$^+$ T cells function

Consistent with several studies, we predicted that TCF4 is a transcription factor for PD-L1 in CRC by JASPAR database: https://jaspar.elixir.no/about, but whether the role of the coactivating transcription factor YAP1 in regulating PD-L1 expression involves TCF4 remains to be further investigated. First, our analysis (Gene Expression Profiling Interactive Analysis [GEPIA: http://gepia.cancer-pku.cn]) revealed that the expression levels of YAP1, TCF4, and PD-L1 were positively correlated with each other in CRC patients. (Figure 5A). Furthermore, CRC patients with higher YAP1 and TCF4 tended to have a shorter disease-free-survival (DFS) than those with lower expression, although the p value was not significant (Figure 5B). Second, we validated that YAP1 and TCF4 positively regulated each other as evaluated by RT-qPCR (Figure 5C) and western blot (Figure 5E). PD-L1 was positively regulated by YAP1 or TCF4 in HCT116 and SW480 cells (Figures 5D, 5E, 5H, and 5I). Interestingly, RT-qPCR and western blotting showed that PD-L1 was more strongly upregulated by co-overexpression of YAP1 and TCF4 than by YAP1 or TCF4 overexpression alone in HCT116 and SW480 cells (Figures 5F and 5G). Third, compared to the negative control group, HCT116 and SW480 cells with upregulated YAP1 or TCF4 inhibited IFN-γ, TNF-α, IL-4, and Granyzm B production by CD8$^+$ T cells (Figures 5J and 5K), and, in turn, HCT116 and SW480 cells with downregulation of YAP1 or TCF4 enhanced IFN-γ, TNF-α, IL-4, and Granyzm B production by CD8$^+$ T cells (Figures 5J and 5K). These results suggest that YAP1 interacts with TCF4 to promote CD8$^+$ T cell dysfunction by regulating PD-L1 levels in tumor cells.

To validate the direct binding of YAP1 and TCF4, we performed a co-immunoprecipitation (coIP) assay. The results showed that the YAP1 antibody enriched the TCF4 protein and the TCF4 antibody enriched the YAP1 protein (Figure 5L). Next, we predicted that the PD-L1 promoter has six potential TCF4 binding sites (http://jaspar.binf.ku.dk). Based on the binding sites, PD-L1 promoter wild-type plasmids (PD-L1-WT), mutant plasmids (PD-L1-MUT), and negative control plasmids were constructed (Figure 5M). We performed dual luciferase reporter gene experiments in 293T cells showing that the TCF4 plasmid enhances PD-L1-WT promoter activity but not PD-L1-MUT (Figure 5N). In addition, the chromatin immunoprecipitation (ChIP) assay was performed using an anti-TCF4 antibody. The results of ChIP-qPCR demonstrated the binding of TCF4 to the PD-L1 promoter (Figure 5O).

## CircYAP1 promotes immune escape as well as metastasis *in vivo*

To investigate the contribution of circYAP1 to immune escape *in vivo*, we constructed HCT116 cell lines stably transfected with lentivirus-negative control (LV-NC) and LV-circYAP1 (Figure 6A). First, stably transfected cells were subcutaneously injected into humanised peripheral blood mononuclear cell (huPBMC)-NOD/Shi-scid-IL2rγ$^{null}$ (NOG)-MHC double knockoff (dKO) mice (Figure 6B). Importantly, the tumor volume and weight were significantly larger in the LV-circYAP1 group than in the LV-NC group (Figures 6C–6F). Moreover, we found more nuclear YAP1 in the LV-circYAP1 group tumors (Figure 6G). IHC of TCF4 and PD-L1 showed that upregulation of circYAP1 significantly increased TCF4 and PD-L1 expression (Figures 6H and 6I). IHC of Ki67 confirmed that overexpression of circYAP1 promoted tumor proliferation (Figure 6J). IHC of CD8 indicated that LV-circYAP1 significantly suppressed the number of infiltrating CD8$^+$ T cells in tumor tissue (Figure 6K). These results demonstrate that overexpression of circYAP1 promotes tumor immune escape as well as proliferation *in vivo*.

In addition, we constructed a nude mouse lung metastasis model by tail vein injection of a stably transfected cells to observe the effect of circYAP1 on metastasis *in vivo* (Figure 7A). After 42 days, lung tissue from the nude mice was collected and made into paraffin sections. The H&E results showed that nude mice in the LV-circYAP1 group had more lung metastatic nodules and larger nodules than those in the LV-NC group (Figures 7B and 7C). IHC of YAP1, TCF4, and PD-L1 showed that metastatic nodes in the LV-circYAP1 group expressed more YAP1, TCF4, and PD-L1 than those in the LV-NC group (Figures 7D–7F). Consistent with the *in vitro* results, overexpression of circYAP1 increased N-cadherin and decreased E-cadherin in the metastatic lung nodules of nude mice (Figures 7G and 7H). The aforementioned data confirm that overexpression of circYAP1 promotes tumor metastasis *in vivo*.

## YTHDF2 promotes m6A-modified circYAP1 degradation

N6-methyladenosine methylation has been reported to be involved in aberrant circRNA expression.[22] To explore the role of m6A in circYAP1 dysregulation, we predicted that m6A modifications are present in circYAP1 (http://www.cuilab.cn/sramp) (Figure 8A). Next, methylated RNA immunoprecipitation (MeRIP)-qPCR results indicated that circYAP1 could be specifically enriched by the anti-m6A antibody in HCT116 cells (Figure 8B). This shows the presence of m6A modifications in circYAP1.

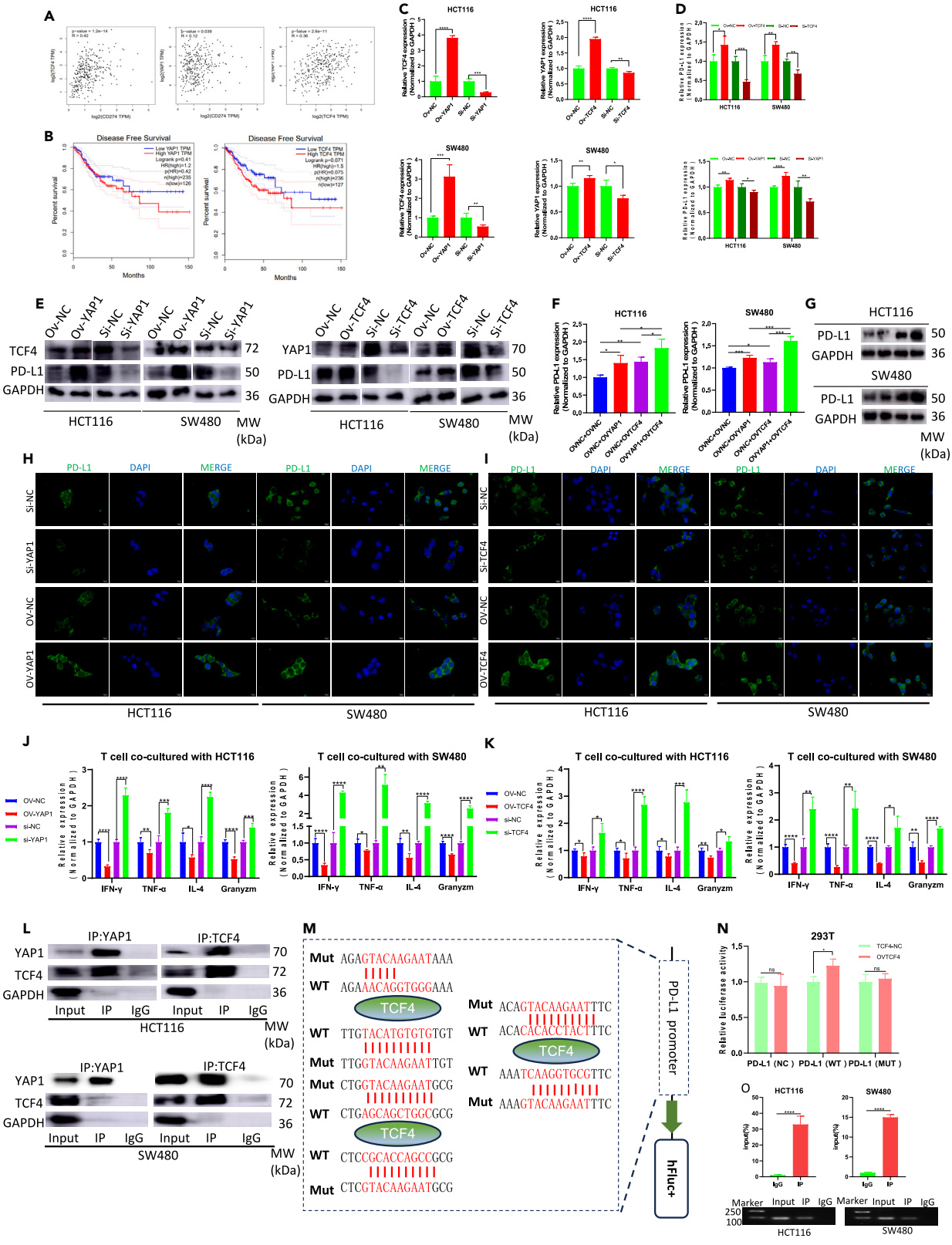
A
B
Disease Free Survival
Disease Free Survival
Months
Months
C
HCT116
SW480
D
HCT116
SW480
E
Ov-NC
Ov-YAP1
Si-NC
Si-YAP1
TCF4
PD-L1
GAPDH
72
50
36
HCT116
SW480
MW (kDa)
Ov-NC
Ov-TCF4
Si-NC
Si-TCF4
YAP1
PD-L1
GAPDH
70
50
36
HCT116
SW480
MW (kDa)
F
HCT116
SW480
Relative PD-L1 expression (Normalized to GAPDH)
OVNC+OVNC
OVNC+OVYAP1
OVNC+OVTCF4
OVYAP1+OVTCF4
G
HCT116
PD-L1
GAPDH
50
36
SW480
PD-L1
GAPDH
50
36
MW (kDa)
H
PD-L1
DAPI
MERGE
Si-NC
Si-YAP1
OV-NC
OV-YAP1
HCT116
SW480
I
PD-L1
DAPI
MERGE
Si-NC
Si-TCF4
OV-NC
OV-TCF4
HCT116
SW480
J
T cell co-cultured with HCT116
T cell co-cultured with SW480
OV-NC
OV-YAP1
si-NC
si-YAP1
Relative expression (Normalized to GAPDH)
IFN-γ
TNF-α
IL-4
Granyzm
K
T cell co-cultured with HCT116
T cell co-cultured with SW480
OV-NC
OV-TCF4
si-NC
si-TCF4
Relative expression (Normalized to GAPDH)
IFN-γ
TNF-α
IL-4
Granyzm
L
IP:YAP1
IP:TCF4
YAP1
TCF4
GAPDH
70
72
36
Input
IP
IgG
HCT116
MW (kDa)
IP:YAP1
IP:TCF4
YAP1
TCF4
GAPDH
70
72
36
Input
IP
IgG
SW480
MW (kDa)
M
Mut AGAGTACAAGAATAAA
WT AGAAACAGGTGGGAAA
TCF4
WT TTGTACATGTGTGTGT
Mut TTGGTACAAGAATTGT
Mut CTGGTACAAGAATGCG
WT CTGAGCAGCTGGCGCG
TCF4
WT CTCCGCACCAGCCGCG
Mut CTCGTACAAGAATGCG
Mut ACAGTACAAGAATTTC
WT ACACACACCTACTTTC
TCF4
WT AAATCAAGGTGCGTTC
Mut AAAGTACAAGAATTTC
PD-L1 promoter
hFluc+
N
293T
TCF4-NC
OVTCF4
Relative luciferase activity
ns
PD-L1 (NC)
PD-L1 (WT)
PD-L1 (MUT)
O
HCT116
SW480
Input(%)
IgG
IP
Marker
Input
IP
IgG
250
100
HCT116
SW480

**Figure 5. YAP1 interactions with TCF4 regulate PD-L1 expression to inhibit CD8$^+$ T cells function**

(A) Correlation analysis between YAP1, TCF4, and PD-L1 in CRC tissue was reanalyzed using GEPIA.

(B) The DFS of YAP1 and TCF4 in CRC patients was reanalyzed using GEPIA.

(C–G) RT-qPCR (n = 4 each group was made in quadruplicate, ANOVA test) and western blot analysis of YAP1, TCF4, and PD-L1 in HCT116 and SW480 cells to verified three of them mutual regulation.

(H and I) IF identified the expression level of PD-1 protein altered by YAP1 and TCF4 in HCT116 and SW480 cells (Scale bar: 10 μm).

(J and K) RT-qPCR identified the expression level of IFN-γ, TNF-α, IL-4, and Granyzm B in CD8$^+$ T cells cocultured with YAP1 or TCF4 expression-altered HCT116 and SW480 cells (n = 4 each group was made in quadruplicate, ANOVA test).

(L) CoIP to analyze the direct binding between YAP1 and TCF4 in HCT116 and SW480 cells.

(M) The schematic diagram depicting the TCF4 binding site on the PD-L1 promoter along with the mutation sequence.

(N) Luciferase activity of 293T transfected with PD-L1 promoter-nc/wt/mut luciferase constructs with TCF4 plasmids or negative control (n = 4 each group was made in quadruplicate, ANOVA test).

(O) ChIP-qPCR to validate the binding of TCF4 to PD-L1 promoter (n = 4 each group was made in quadruplicate, unpaired t test). Data are expressed as mean ± standard deviation, ns $p \geq 0.05$, *$p < 0.05$, **$p < 0.01$, ***$p < 0.001$, ****$p < 0.0001$.

YTHDF2 is one of the primary components in the biological function of m6A modifications.[23] YTHDF2 recognizes and binds m6A-modified mRNAs and exerts tumor suppressive activity by promoting targeted mRNA degradation.[24–26] To assess the regulatory value of YTHDF2 on circYAP1 in HCT116 cells, we synthesized siRNA and overexpression plasmids targeting YTHDF2. We confirmed the high efficacy of the siRNA and plasmid by RT-qPCR in HCT116 cells (Figure 8C). The results showed that siYTHDF2 increased circYAP1 expression in HCT116 cells, while the YTHDF2 overexpression plasmid decreased the circYAP1 expression in HCT116 cells (Figure 8D). Moreover, we found that overexpressed YTHDF2 promoted the degradation of circYAP1 in HCT116 cells by actinomycin D assay (Figure 8E).

To study the regulatory mechanism of YTHDF2 on circYAP1, we used FISH-IF to observe their distribution. FISH-IF showed that the circYAP1 and YTHDF2 proteins had partially overlapping positions in HCT116 cells (Figure 8F). Next, RIP-qPCR showed that circYAP1 is pulled down more in the ov-circYAP1 group than in the overexpression-negative control (ov-nc) group by the YTHDF2 antibody in HCT116 cells (Figure 8G). Moreover, in circYAP1-overexpressing HCT116 cells, YTHDF2 was enriched by the circ YAP1 probe but not the NC probe (Figure 8H). These results suggest that YTHDF2 can bind circYAP1 to degrade it.

## DISCUSSION

In recent years, aberrant circRNAs have been shown to be involved in tumor immune escape.[27] In this study, we mainly provided a more insightful exploration of the function and mechanism of circYAP1 in CRC immune escape. We found that circYAP1 was significantly upregulated in CRC and had the potential to serve as a biomarker for CRC patients prognosis. *In vitro* and *in vivo* experiments showed that circYAP1 exerted an effect on CRC cell proliferation, migration, invasion, and especially immune evasion by activating the YAP1/TCF4-PD-L1 axis.

CircRNAs usually function as competing endogenous RNAs and RBPs and encode polypeptides. The role of circRNA in tumor immune escape and immunotherapeutic response is gradually being explored. CircDLG1 increased infiltration of myeloid-derived suppressor cells (MDSCs) into gastric cancer tissues, leading to tumor immune evasion.[28] In melanoma, circ_0020710 resulted in the exhaustion of cytotoxic lymphocytes and resistance to anti-PD-1 therapy by upregulating CXCL12.[29] Knockdown of circFAT1 improved the sensitivity of PD1 blockade therapy by enhancing CD8$^+$ T cell infiltration into head and neck squamous cell carcinoma tissues.[10] In our study, we found that circYAP1 inhibited the expression of IFN-γ, TNF-α, IL-4, and Granyzm B in CD8$^+$ T cells by upregulating tumor cell PD-L1, leading to CRC immune evasion.

PD-L1 is one of the best known immune checkpoints.[30] Multiple factors regulate PD-L1, which helps cancer cells evade the immune system.[31] The deubiquitination of PD-L1 inhibited the treatment efficacy of anti-PD-1 therapy in lung cancer.[32] Acetylated PD-L1 enters the nucleus to promote the expression of immune response-related genes affecting the efficacy of anti-PD-1 immunotherapy.[12] Moreover, multiple classical signaling pathways regulate PD-L1 expression, such as the nuclear factor κB (NF-κB) pathway,[33] janus tyrosine kinase-signal transducer and activator of transcription (JAK-STAT) pathway,[34] and wingless integrated (WNT) pathway.[35] In addition, evidence that circRNAs regulate PD-L1 expression is increasingly being uncovered. Circ_0000052 targeted miR-382-3p and attenuated its inhibition of PD-L1 in head and neck squamous cell carcinoma.[36] In the hypoxic microenvironment of hepatocellular carcinoma, circPRDM4 recruited HIF-1α to the PD-L1 promoter region and promoted PD-L1 upregulation.[37] Similarly, we found that circYAP1 increased PD-L1 expression by promoting its transcription in CRC. Mechanically, circYAP1 did not phosphorylate the YAP1 protein but rather translocated the active form of YAP1 into the nucleus. YAP1 must bind to other transcription factors (TEAD, TCF4, etc.) to exert transcription factor activity. We found that YAP1 directly bound to TCF4 to promote PD-L1 promoter transcription. Moreover, YAP1 and TCF4 synergistically control of PD-L1 expression in CRC cells to inhibit expression of IFN-γ, TNF-α, IL-4, and Granyzm B in CD8$^+$ T cells.

In recent years, the nonimmune checkpoint role of PD-L1 has gradually received attention. PD-L1 promoted stem cell proliferation and survival through changes in glucose metabolism and fatty acid metabolism in leukemia cells.[38] In acute myeloid leukemia, PD-L1 activated the PI3K-AKT signaling pathway to regulate cell proliferation and apoptosis.[39] PD-L1 promoted invasion and metastasis in ovarian cancer.[40] In our study, we explored both the immune checkpoint and nonimmune checkpoint roles of PD-L1 in CRC. Functional assays have shown that knockdown of PD-L1 attenuates the proliferation, migration, and invasion of CRC cells. Our rescue results showed that circYAP1 can promote CRC proliferation, migration, and invasion, especially immune evasion, depending on PD-L1. Interestingly, we found that, although high expression of PD-L1 predicts poor prognosis, patients with high PD-L1 expression tend to be more sensitive to immunotherapy and survive

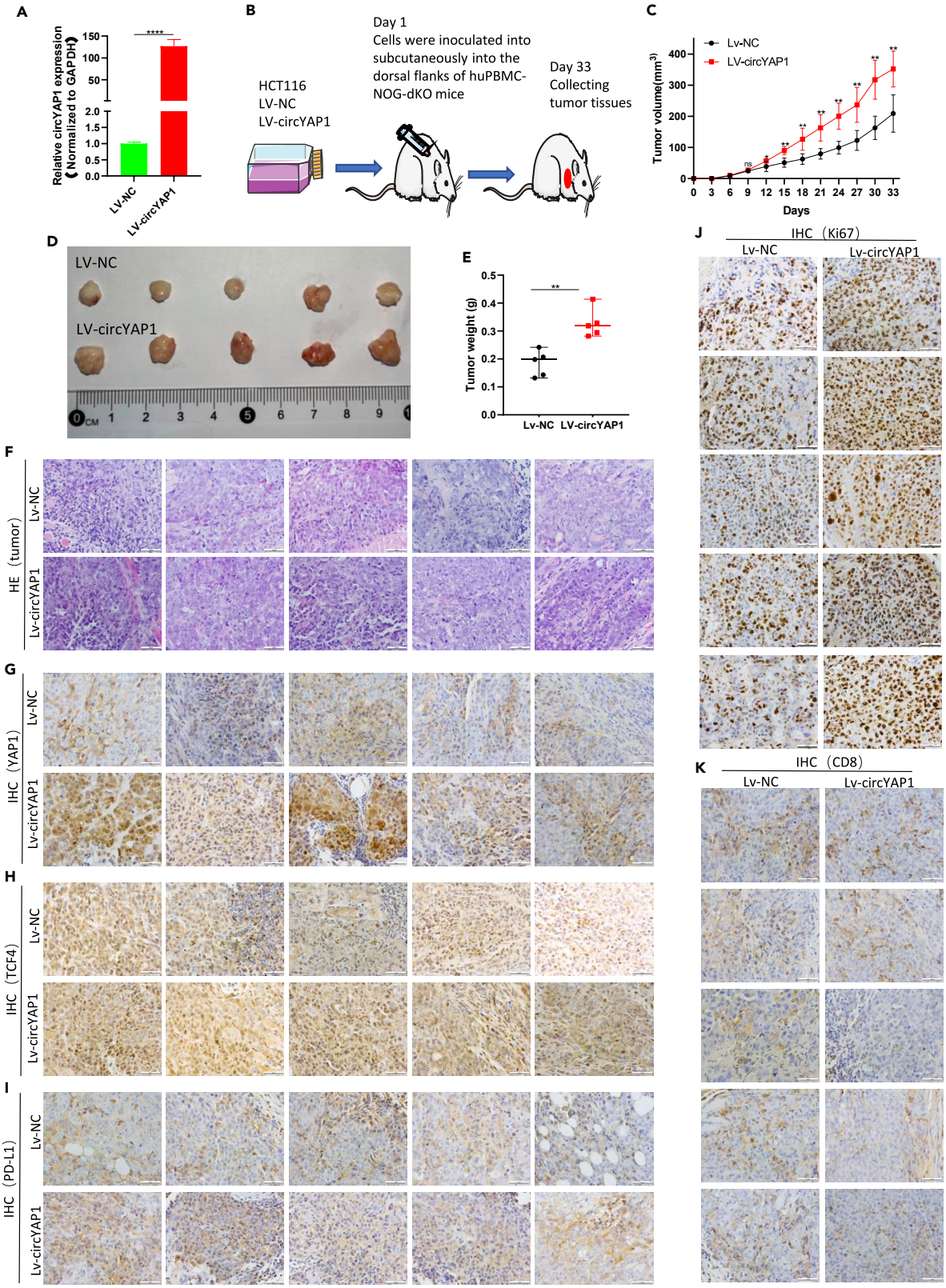
A
Relative circYAP1 expression (Normalized to GAPDH)
LV-NC
LV-circYAP1
B
HCT116
LV-NC
LV-circYAP1
Day 1
Cells were inoculated into subcutaneously into the dorsal flanks of huPBMC-NOG-dKO mice
Day 33
Collecting tumor tissues
C
Lv-NC
LV-circYAP1
Tumor volume(mm3)
Days
D
LV-NC
LV-circYAP1
E
Tumor weight (g)
Lv-NC LV-circYAP1
F
HE (tumor)
Lv-NC
Lv-circYAP1
G
IHC (YAP1)
H
IHC (TCF4)
I
IHC (PD-L1)
J
IHC (Ki67)
K
IHC (CD8)

**Figure 6. circYAP1 promotes immune escape *in vivo***

(A) Overexpression efficiency of circYAP1 in stable cell line of HCT116.

(B) Schematic diagram of the construction of a subcutaneous xenograft tumor in huPBMC-NOG-dKO mice.

(C) Growth curves of xenograft tumors measured every 3 days (n = 5 mice per group, unpaired t test).

(D and E) Images of xenograft tumors of each group and weight of them measured at day 33(n = 5 mice per group, unpaired t test).

(F) HE staining of subcutaneous xenograft tumor (Scale bar: 50 μm) (G, H, I) Relative protein levels of YAP1, TCF4, PD-L1 were detected in lung metastatic nodules by ISH (Scale bar: 50 μm).

(J and K) Ki-67-positive tumor cells and CD8-positive T cells infiltrated in the tumor detected by ISH (Scale bar: 50 μm). Data are expressed as mean ± standard deviation, ns $p \geq 0.05$, *$p < 0.05$, **$p < 0.01$, ****$p < 0.0001$.

longer after immunotherapy than patients with low PD-L1 expression. The reason for this paradox may be related to the increase in targets for immunotherapy. This also suggests that a great deal of exploration is needed from basic research to clinical translation.

Recent reports suggest that YTHDF2 can promote m6A-mRNA degradation in various diseases.[41] These mRNAs may promote or mitigate tumor progression.[42,43] In this study, we found the presence of an m6A modification on circYAP1 and that YTHDF2 overexpression could target m6A-circYAP1 to promote degradation in HCT116 cells. However, whether YTHDF2 regulates the immune response via m6A-circRNA requires solid supportive data support, and this is where our future research will be directed.

## Conclusion

In brief, we found that circYAP1 was significantly upregulated in the CRC tissues. CircYAP1 promoted CRC cell proliferation, invasion, migration, and immune escape by upregulating PD-L1 in CRC cells. Mechanistically, we found that circYAP1 directly binds to the YAP1 protein to prevent its phosphorylation, inducing the transport of YAP1 into the nucleus, and YAP1 initiates PD-L1 transcription by interacting with TCF4. Moreover, we found that YTHDF2 regulates the degradation of circYAP1 by recognizing the m6A modification of circYAP1. This study provides an insight into circRNA-induced immune escape mechanisms and can provide a new target for combination immunotherapy.

## Limitations of the study

However, no circYAP1 expression data of CRC patients treated with anti-PD1/PD-L1 therapy have been disclosed, so the correlation of circYAP1 and therapeutic efficacy cannot be performed so far. We will conduct clinical validation in future studies to demonstrate that circYAP1 can predict immunotherapy outcomes in CRC patients. This will enable clinical translation of the significance of circYAP1.

## STAR★METHODS

Detailed methods are provided in the online version of this paper and include the following:

- KEY RESOURCES TABLE
- RESOURCE AVAILABILITY
  - Lead contact
  - Materials availability
  - Data and code availability
- EXPERIMENTAL MODEL AND SUBJECT DETAILS
  - Clinical specimens
  - Cell lines
  - Animals
  - Statement of ethics
- METHOD DETAILS
  - Cell transfection of siRNAs and plasmids
  - Total RNA isolation, reverse transcription and qRT-PCR
  - RNase R treatment and actinomycin D assay
  - RNA *in-situ* hybridization (ISH) and fluorescence *in-situ* hybridization (FISH)
  - Western blot analysis, immunofuorescence (IF), and immunohistochemistry (IHC)
  - CCK-8, EDU, migration and invasion assays
  - $CD8^+$ T cells isolation and incubation with CRC cells
  - RNA pull-down assay, RNA immunoprecipitation (RIP) and co-IP
  - Dual luciferase reporter assay
  - Animal models
- QUANTIFICATION AND STATISTICAL ANALYSIS

## SUPPLEMENTAL INFORMATION

Supplemental information can be found online at https://doi.org/10.1016/j.isci.2023.108779.

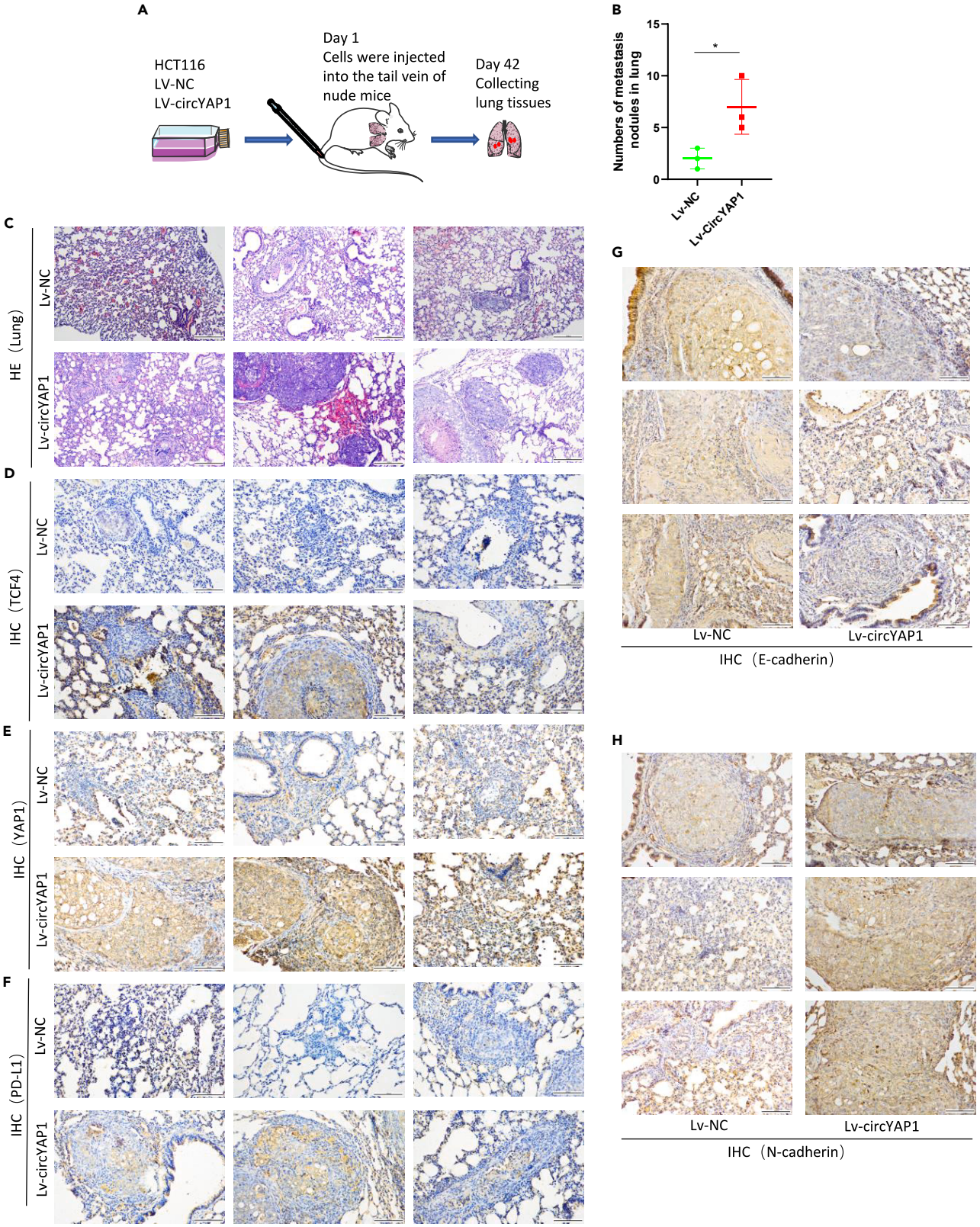
A
HCT116
LV-NC
LV-circYAP1
Day 1
Cells were injected into the tail vein of nude mice
Day 42
Collecting lung tissues
B
Numbers of metastasis nodules in lung
15
10
5
0
*
Lv-NC
Lv-CircYAP1
C
HE（Lung）
Lv-NC
Lv-circYAP1
D
IHC（TCF4）
Lv-NC
Lv-circYAP1
E
IHC（YAP1）
Lv-NC
Lv-circYAP1
F
IHC（PD-L1）
Lv-NC
Lv-circYAP1
G
Lv-NC
Lv-circYAP1
IHC（E-cadherin）
H
Lv-NC
Lv-circYAP1
IHC（N-cadherin）

**Figure 7. circYAP1 promotes lung metastasis *in vivo***

(A) Schematic diagram of the construction of a lung metastasis model in nude mice.

(B) The number of lung metastasis nodules in lv-circYAP1 and lv-nc group nude mice (n = 3 mice per group, unpaired t test).

(C) HE staining of lung metastatic nodules (Scale bar: 200 μm) (D, E, F, G, H) Relative protein levels of YAP1, TCF4, PD-L1, E-cadherin, and N-cadherin were detected in lung metastatic nodules by ISH (Scale bar: 200 μm). Data are expressed as mean ± standard deviation, *p < 0.05.

## ACKNOWLEDGMENTS

We offer special thanks to Zaoqu Liu (The First Affiliated Hospital of Zhengzhou University), and all the members of his team, RookieUtopia, for developing the BEST application (https://rookieutopia.com/). This study was supported by the National Natural Science Foundation of China (81972663, 82173055), Scientific Research and Innovation Team of The First Affiliated Hospital of Zhengzhou University (ZYCXTD2023017), The Excellent Youth Science Project of Henan Natural Science Foundation (212300410074), The Youth Talent Innovation Team Support Program of Zhengzhou University (32320290), the Provincial and Ministry Co-constructed Key Projects of Henan Medical Science and Technology

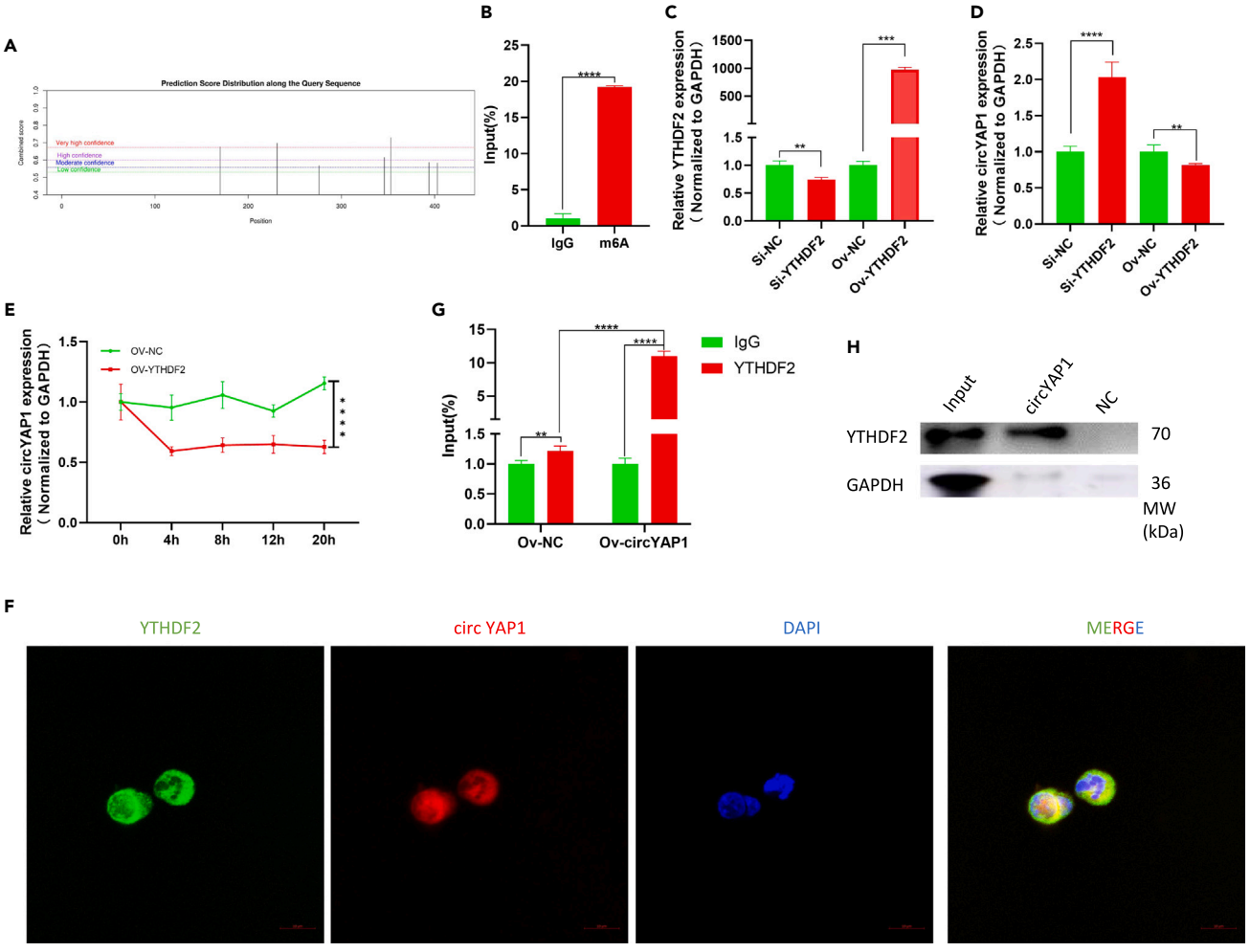


**Figure 8. YTHDF2 promotes m6A-modified circYAP1 to degradation**

(A) The m6A modification of circYAP1 is predicted by SRAMP (http://www.cuilab.cn/sramp).

(B) The m6A modification of circYAP1 was confirmed by MeRIP-qPCR (n = 4 each group was made in quadruplicate, unpaired t test).

(C and D) RT-qPCR analysis of YTHDF2 and circYAP1 expression level in HCT116 cells transfected with YTHDF2 plasmids and negative control (n = 4 each group was made in quadruplicate, unpaired t test).

(E) The abundance of circYAP1 in overexpressed-YTHDF2 HCT116 cells cultured with actinomycin D at 0, 4, 8, 12, and 20 h was analyzed by RT-qPCR (n = 4 each group was made in quadruplicate, unpaired t test).

(F–H) Direct binding between circYAP1 and YTHDF2 was confirmed by FISH-IF colocalization (Scale bar: 10 μm), RIP-PCR (n = 4 each group was made in quadruplicate, unpaired t test), and RNA pull-down experiments in HCT116 cells. Data are expressed as mean ± standard deviation, **p < 0.01, ***p < 0.001, ****p < 0.0001.

(SBGJ202102134), Henan Medical Technology Popularization Project (SYJS2022109), Henan Provincial Health and Health Commission Joint Construction Project (LHGJ20200158), and Henan Province Young and Middle-aged Health Science and Technology Innovation Leading Talent Project (YXKC2022016).

## DECLARATION OF INTERESTS

The authors declare no competing interests.

## AUTHOR CONTRIBUTIONS

Z.S., Y.L., and C.W. provided direction and guidance throughout the preparation of this manuscript. Z.C. and W.W. conducted experiments and wrote and edited the manuscript. S.H., H.S., and C.C. collected tissue samples. Z.Z. and X.S. reviewed and made significant revisions to the manuscript. B.J. and J.H. collected and prepared the related papers. All authors read and approved the final manuscript.

Received: July 20, 2023
Revised: October 20, 2023
Accepted: December 26, 2023
Published: December 30, 2023

## REFERENCES

1. Cai, Z., and Liu, Q. (2021). Understanding the Global Cancer Statistics 2018: implications for cancer control. Sci. China Life Sci. *64*, 1017–1020.
2. Feng, R.M., Zong, Y.N., Cao, S.M., and Xu, R.H. (2019). Current cancer situation in China: good or bad news from the 2018 Global Cancer Statistics? Cancer Commun. *39*, 22.
3. Bray, F., Ferlay, J., Soerjomataram, I., Siegel, R.L., Torre, L.A., and Jemal, A. (2018). Global cancer statistics 2018: GLOBOCAN estimates of incidence and mortality worldwide for 36 cancers in 185 countries. CA. Cancer J. Clin. *68*, 394–424.
4. Wang, Y., Li, C., Wang, Z., Wang, Z., Wu, R., Wu, Y., Song, Y., and Liu, H. (2022). Comparison between immunotherapy efficacy in early non-small cell lung cancer and advanced non-small cell lung cancer: a systematic review. BMC Med. *20*, 426.
5. Crommentuijn, M.H.W., Schetters, S.T.T., Dusoswa, S.A., Kruijssen, L.J.W., Garcia-Vallejo, J.J., and van Kooyk, Y. (2020). Immune involvement of the contralateral hemisphere in a glioblastoma mouse model. J. Immunother. Cancer *8*, e000323.
6. Adinew, G.M., Messeha, S.S., Taka, E., Badisa, R.B., and Soliman, K.F.A. (2022). Anticancer Effects of Thymoquinone through the Antioxidant Activity, Upregulation of Nrf2, and Downregulation of PD-L1 in Triple-Negative Breast Cancer Cells. Nutrients *14*, 4787.
7. Sidibe, A., Ropraz, P., Jemelin, S., Emre, Y., Poittevin, M., Pocard, M., Bradfield, P.F., and Imhof, B.A. (2018). Angiogenic factor-driven inflammation promotes extravasation of human proangiogenic monocytes to tumours. Nat. Commun. *9*, 355.
8. Young, T.M., Reyes, C., Pasnikowski, E., Castanaro, C., Wong, C., Decker, C.E., Chiu, J., Song, H., Wei, Y., Bai, Y., et al. (2020). Autophagy protects tumors from T cell-mediated cytotoxicity via inhibition of TNFalpha-induced apoptosis. Sci. Immunol. *5*, eabb9561.
9. Costamagna, D., Duelen, R., Penna, F., Neumann, D., Costelli, P., and Sampaolesi, M. (2020). Interleukin-4 administration improves muscle function, adult myogenesis, and lifespan of colon carcinoma-bearing mice. J. Cachexia Sarcopenia Muscle *11*, 783–801.
10. Jia, L., Wang, Y., and Wang, C.Y. (2021). circFAT1 Promotes Cancer Stemness and Immune Evasion by Promoting STAT3 Activation. Adv. Sci. *8*, 2003376.
11. Xiong, W., Gao, X., Zhang, T., Jiang, B., Hu, M.M., Bu, X., Gao, Y., Zhang, L.Z., Xiao, B.L., He, C., et al. (2022). USP8 inhibition reshapes an inflamed tumor microenvironment that potentiates the immunotherapy. Nat. Commun. *13*, 1700.
12. Gao, Y., Nihira, N.T., Bu, X., Chu, C., Zhang, J., Kolodziejczyk, A., Fan, Y., Chan, N.T., Ma, L., Liu, J., et al. (2020). Acetylation-dependent regulation of PD-L1 nuclear translocation dictates the efficacy of anti-PD-1 immunotherapy. Nat. Cell Biol. *22*, 1064–1075.
13. Xiong, W., Gao, Y., Wei, W., and Zhang, J. (2021). Extracellular and nuclear PD-L1 in modulating cancer immunotherapy. Trends Cancer *7*, 837–846.
14. Janse van Rensburg, H.J., Azad, T., Ling, M., Hao, Y., Snetsinger, B., Khanal, P., Minassian, L.M., Graham, C.H., Rauh, M.J., and Yang, X. (2018). The Hippo Pathway Component TAZ Promotes Immune Evasion in Human Cancer through PD-L1. Cancer Res. *78*, 1457–1470.
15. Miao, J., Hsu, P.C., Yang, Y.L., Xu, Z., Dai, Y., Wang, Y., Chan, G., Huang, Z., Hu, B., Li, H., et al. (2017). YAP regulates PD-L1 expression in human NSCLC cells. Oncotarget *8*, 114576–114587.
16. Wu, A., Wu, Q., Deng, Y., Liu, Y., Lu, J., Liu, L., Li, X., Liao, C., Zhao, B., and Song, H. (2019). Loss of VGLL4 suppresses tumor PD-L1 expression and immune evasion. EMBO J. *38*, e99506.
17. Wang, J., Zhao, X., Wang, Y., Ren, F., Sun, D., Yan, Y., Kong, X., Bu, J., Liu, M., and Xu, S. (2020). circRNA-002178 act as a ceRNA to promote PDL1/PD1 expression in lung adenocarcinoma. Cell Death Dis. *11*, 32.
18. Chen, C., Yuan, W., Zhou, Q., Shao, B., Guo, Y., Wang, W., Yang, S., Guo, Y., Zhao, L., Dang, Q., et al. (2021). N6-methyladenosine-induced circ1662 promotes metastasis of colorectal cancer by accelerating YAP1 nuclear localization. Theranostics *11*, 4298–4315.
19. Juneja, V.R., McGuire, K.A., Manguso, R.T., LaFleur, M.W., Collins, N., Haining, W.N., Freeman, G.J., and Sharpe, A.H. (2017). PD-L1 on tumor cells is sufficient for immune evasion in immunogenic tumors and inhibits CD8 T cell cytotoxicity. J. Exp. Med. *214*, 895–904.
20. Eichberger, J., Schulz, D., Pscheidl, K., Fiedler, M., Reichert, T.E., Bauer, R.J., and Ettl, T. (2020). PD-L1 Influences Cell Spreading, Migration and Invasion in Head and Neck Cancer Cells. Int. J. Mol. Sci. *21*, 8089.
21. Wang, H., Zhang, H., Sun, Z., Chen, W., and Miao, C. (2021). GABAB receptor inhibits tumor progression and epithelial-mesenchymal transition via the regulation of Hippo/YAP1 pathway in colorectal cancer. Int. J. Biol. Sci. *17*, 1953–1962.
22. Liu, Y., Yang, Y., Lin, Y., Wei, B., Hu, X., Xu, L., Zhang, W., and Lu, J. (2023). N(6) -methyladenosine-modified circRNA RERE modulates osteoarthritis by regulating beta-catenin ubiquitination and degradation. Cell Prolif. *56*, e13297.
23. Lu, M., Zhang, Z., Xue, M., Zhao, B.S., Harder, O., Li, A., Liang, X., Gao, T.Z., Xu, Y., Zhou, J., et al. (2020). N(6)-methyladenosine modification enables viral RNA to escape recognition by RNA sensor RIG-I. Nat. Microbiol. *5*, 584–598.
24. Fang, R., Chen, X., Zhang, S., Shi, H., Ye, Y., Shi, H., Zou, Z., Li, P., Guo, Q., Ma, L., et al. (2021). EGFR/SRC/ERK-stabilized YTHDF2 promotes cholesterol dysregulation and invasive growth of glioblastoma. Nat. Commun. *12*, 177.
25. Xu, P., Hu, K., Zhang, P., Sun, Z.G., and Zhang, N. (2022). Hypoxia-mediated YTHDF2 overexpression promotes lung squamous cell carcinoma progression by activation of the mTOR/AKT axis. Cancer Cell Int. *22*, 13.
26. Zhou, Y., Fan, K., Dou, N., Li, L., Wang, J., Chen, J., Li, Y., and Gao, Y. (2023). YTHDF2 exerts tumor-suppressor roles in gastric cancer via up-regulating PPP2CA independently of m(6)A modification. Biol. Proced. Online *25*, 6.
27. Chen, Y., Li, Z., Liang, J., Liu, J., Hao, J., Wan, Q., Liu, J., Luo, C., and Lu, Z. (2022). CircRNA has_circ_0069313 induced OSCC immunity escape by miR-325-3p-Foxp3 axes in both

OSCC cells and Treg cells. Aging (Albany NY) *14*, 4376–4389.

28. Chen, D.L., Sheng, H., Zhang, D.S., Jin, Y., Zhao, B.T., Chen, N., Song, K., and Xu, R.H. (2021). The circular RNA circDLG1 promotes gastric cancer progression and anti-PD-1 resistance through the regulation of CXCL12 by sponging miR-141-3p. Mol. Cancer *20*, 166.
29. Wei, C.Y., Zhu, M.X., Lu, N.H., Liu, J.Q., Yang, Y.W., Zhang, Y., Shi, Y.D., Feng, Z.H., Li, J.X., Qi, F.Z., and Gu, J.Y. (2020). Circular RNA circ_0020710 drives tumor progression and immune evasion by regulating the miR-370-3p/CXCL12 axis in melanoma. Mol. Cancer *19*, 84.
30. Song, L., Liu, S., and Zhao, S. (2022). Everolimus (RAD001) combined with programmed death-1 (PD-1) blockade enhances radiosensitivity of cervical cancer and programmed death-ligand 1 (PD-L1) expression by blocking the phosphoinositide 3-kinase (PI3K)/protein kinase B (AKT)/mammalian target of rapamycin (mTOR)/S6 kinase 1 (S6K1) pathway. Bioengineered *13*, 11240–11257.
31. Zhang, J., Zhang, G., Zhang, W., Bai, L., Wang, L., Li, T., Yan, L., Xu, Y., Chen, D., Gao, W., et al. (2022). Loss of RBMS1 promotes anti-tumor immunity through enabling PD-L1 checkpoint blockade in triple-negative breast cancer. Cell Death Differ. *29*, 2247–2261.
32. Liu, Z., Wang, T., She, Y., Wu, K., Gu, S., Li, L., Dong, C., Chen, C., and Zhou, Y. (2021). N(6)-methyladenosine-modified circIGF2BP3 inhibits CD8(+) T-cell responses to facilitate tumor immune evasion by promoting the deubiquitination of PD-L1 in non-small cell lung cancer. Mol. Cancer *20*, 105.
33. Cai, H., Yan, L., Liu, N., Xu, M., and Cai, H. (2020). IFI16 promotes cervical cancer progression by upregulating PD-L1 in immunomicroenvironment through STING-TBK1-NF-kB pathway. Biomed. Pharmacother. *123*, 109790.
34. Song, T.L., Nairismägi, M.L., Laurensia, Y., Lim, J.Q., Tan, J., Li, Z.M., Pang, W.L., Kizhakeyil, A., Wijaya, G.C., Huang, D.C., et al. (2018). Oncogenic activation of the STAT3 pathway drives PD-L1 expression in natural killer/T-cell lymphoma. Blood *132*, 1146–1158.
35. Yang, M., Li, Z., Tao, J., Hu, H., Li, Z., Zhang, Z., Cheng, F., Sun, Y., Zhang, Y., Yang, J., et al. (2021). Resveratrol induces PD-L1 expression through snail-driven activation of Wnt pathway in lung cancer cells. J. Cancer Res. Clin. Oncol. *147*, 1101–1113.
36. Zhang, D.J., Fu, Z.M., Guo, Y.Y., Guo, F., Wan, Y.N., and Guan, G.F. (2023). Circ_0000052/miR-382-3p axis induces PD-L1 expression and regulates cell proliferation and immune evasion in head and neck squamous cell carcinoma. J. Cell Mol. Med. *27*, 113–126.
37. Chen, Z.Q., Zuo, X.L., Cai, J., Zhang, Y., Han, G.Y., Zhang, L., Ding, W.Z., Wu, J.D., and Wang, X.H. (2023). Hypoxia-associated circPRDM4 promotes immune escape via HIF-1alpha regulation of PD-L1 in hepatocellular carcinoma. Exp. Hematol. Oncol. *12*, 17.
38. Soltani, M., Ghanadian, M., Ghezelbash, B., Shokouhi, A., Zamyatnin, A.A., Jr., Bazhin, A.V., and Ganjalikhani-Hakemi, M. (2023). PD-L1 stimulation can promote proliferation and survival of leukemic cells by influencing glucose and fatty acid metabolism in acute myeloid leukemia. BMC Cancer *23*, 447.
39. Wang, F., Yang, L., Xiao, M., Zhang, Z., Shen, J., Anuchapreeda, S., Tima, S., Chiampanichayakul, S., and Xiao, Z. (2022). PD-L1 regulates cell proliferation and apoptosis in acute myeloid leukemia by activating PI3K-AKT signaling pathway. Sci. Rep. *12*, 11444.
40. Shen, X., Jin, X., Fang, S., and Chen, J. (2023). EFEMP2 upregulates PD-L1 expression via EGFR/ERK1/2/c-Jun signaling to promote the invasion of ovarian cancer cells. Cell. Mol. Biol. Lett. *28*, 53.
41. Chen, Y., Wang, Y.L., Qiu, K., Cao, Y.Q., Zhang, F.J., Zhao, H.B., and Liu, X.Z. (2022). YTHDF2 promotes temozolomide resistance in glioblastoma by activation of the Akt and NF-kappaB signalling pathways via inhibiting EPHB3 and TNFAIP3. Clin. Transl. Immunology *11*, e1393.
42. Hu, B.B., Wang, X.Y., Gu, X.Y., Zou, C., Gao, Z.J., Zhang, H., and Fan, Y. (2019). N(6)-methyladenosine (m(6)A) RNA modification in gastrointestinal tract cancers: roles, mechanisms, and applications. Mol. Cancer *18*, 178.
43. Chai, R.C., Chang, Y.Z., Chang, X., Pang, B., An, S.Y., Zhang, K.N., Chang, Y.H., Jiang, T., and Wang, Y.Z. (2021). YTHDF2 facilitates UBXN1 mRNA decay by recognizing METTL3-mediated m(6)A modification to activate NF-kappaB and promote the malignant progression of glioma. J. Hematol. Oncol. *14*, 109.
44. Duan, X., Xu, X., Zhang, Y., Gao, Y., Zhou, J., and Li, J. (2022). DDR1 functions as an immune negative factor in colorectal cancer by regulating tumor-infiltrating T cells through IL-18. Cancer Sci. *113*, 3672–3685.

## STAR★METHODS

### KEY RESOURCES TABLE

| REAGENT or RESOURCE | SOURCE | IDENTIFIER |
|---|---|---|
| **Antibodies** | | |
| GAPDH Monoclonal antibody | Proteintech | Cat# 60004-1-Ig; RRID: AB_2107436 |
| E-cadherin Polyclonal antibody | Proteintech | Cat# 20874-1-AP; RRID: AB_10697811 |
| Histone-H3 Polyclonal antibody | Proteintech | Cat# 17168-1-AP; RRID: AB_2716755 |
| TCF4 Polyclonal antibody | Proteintech | Cat# 22337-1-AP; RRID: AB_2879076 |
| Recombinant Anti-PD-L1 antibody | Abcam | Cat# ab213524; RRID: AB_2857903 |
| Recombinant Anti-PD1 antibody | Abcam | Cat# ab137132; RRID: AB_2894867 |
| Recombinant Anti-Interferon gamma antibody | Abcam | Cat# ab231036; RRID: AB_2941995 |
| Recombinant Anti-CD8 alpha antibody | Abcam | Cat# ab245118; RRID: AB_3068617 |
| YAP (D8H1X) XP Rabbit mAb | Cell Signaling Technology | Cat# 14074; RRID: AB_2650491 |
| Phospho-YAP (Ser127) (D9W2I) Rabbit mAb | Cell Signaling Technology | Cat# 13008; RRID: AB_2650553 |
| YTHDF2 (E2I2H) Rabbit mAb | Cell Signaling Technology | Cat# NO.71283; RRID: AB_3068618 |
| m6A antibody | Synaptic Systems | Cat# 202 003; RRID: AB_2279214 |
| Anti -N Cadherin Rabbit pAb | Servicebio | Cat# GB111009-100; RRID: AB_3068619 |
| **Bacterial and virus strains** | | |
| Si-NC | RiboBio | Cat# siN0000001-1-5 |
| si-h-circYAP1_001 (5′ to 3′): AGATGGATACAGCCATGAA | RiboBio | Cat# siB171025053732 |
| si-h-circYAP1_002 (5′ to 3′): TGGATACAGCCATGAACCA | RiboBio | Cat# siB171025053737 |
| si-h-YAP1_020 (5′ to 3′): TGTGGATGAGATGGATACA | RiboBio | Cat# siB160602113946 |
| si-h-TCF4_020 (5′ to 3′): CCATGGAGGTACAGACAAA | RiboBio | Cat# siG1082132427 |
| Si-h-YTHDF2_ 001 (5′ to 3′): GATGGATTACGATGATGAT | RiboBio | Cat# siG141112154420 |
| si-h-CD274_005 (5′ to 3′): CCACCAATTCCAAGAGAGA | RiboBio | Cat# siG150520101800 |
| **Biological samples** | | |
| CRC tissue | The First Affiliated Hospital of Zhengzhou University | N/A |
| **Chemicals, peptides, and recombinant proteins** | | |
| RNAiso Plus | Takara | Cat# 9108 |
| ueIris RT mix with DNase (All-in-One) | US Everbright | Cat# R2020 |
| Cell Counting Kit-8 | Dojindo Laboratories | Cat# CK04 |
| RNase R | Lucigen | Cat# RNR07250 |
| actinomycin D | Merck | Cat# SBR00013 |
| protease inhibitors | Beyotime | Cat# P1005 |
| phosphatase inhibitors | Beyotime | Cat# P1081 |
| RNase inhibitor | ThermoFisher | Cat# 87785 |
| Anti-fluorescence quenching sealing solution (with DAPI) | Beyotime | Cat# P0131-5ml |
| 4% paraformaldehyde | Beyotime | Cat# P0099-500ml |

(*Continued on next page*)

*Continued*

| REAGENT or RESOURCE | SOURCE | IDENTIFIER |
|---|---|---|
| Lipofectamine™ 3000 | Invitrogen | Cat# L3000075 |
| crystal violet | Solarbio | Cat# G1063 |
| Human Recombinant IL-2(CHO-expressed) | STEMCELL Technologies | Cat# 78036.1 |
| ImmunoCultTm Human CD3/CD28/CD2 T Cell Activator | STEMCELL Technologies | Cat# 10970 |
| HieffTrans™ Liposome Transfection Reagent | Yeasen Biotechnology | Cat# 40802ES03 |
| **Critical commercial assays** | | |
| Hieff qPCR SYBR Green Master Mix kit | Yeasen Biotechnology | Cat# 11201ES08 |
| Cell-Light EdU Apollo567 *In Vitro* Kit | RiboBio | Cat# C10310 |
| RNASweAMI™ *In situ* hybridisation DAB test kit | Servicebio | Cat# GF001-50T |
| Easy-Sep™ Direct Human $CD8^+$ T Cell Isolation Kit | STEMCELL Technologies | Cat# 19663 |
| RNA pulldown kit | BersinBio | Cat# Bes5102 |
| Chromatin immunoprecipitation kit | BersinBio | Cat# Bes5001 |
| Magna RIP RNA-Binding Protein Immunoprecipitation Kit | Millipore | Cat# 17-701 |
| Immunoprecipitation kit | Abcam | Cat# ab206996 |
| **Deposited data** | | |
| Transcriptome arrays of CRC tissues | This paper | GEO: GSE106584; GEO: GSE87211; GEO: GSE19750 |
| **Experimental models: Cell lines** | | |
| HCT116 | Shanghai Cell Bank of Chinese Academy of Sciences | Cat# TCHu99 |
| SW480 | Shanghai Cell Bank of Chinese Academy of Sciences | Cat# TCHu172 |
| Human embryonic kidney 293 T cells | Shanghai Cell Bank of Chinese Academy of Sciences | Cat# SCSP-502 |
| Human CD8 T cells | Isolated from peripheral blood | N/A |
| **Experimental models: Organisms/strains** | | |
| BALB/c nude mice | Vital River Laboratory | N/A |
| huPBMC-NOG-dKO mice | Vital River Laboratory | N/A |
| **Oligonucleotides** | | |
| Primers used in this study, see Table S1 | This paper | N/A |
| CircYAP FISH probe: mTmTCmAmTGGCmTGm TmAmTCCmAmTCmTCmAmTCCmA | GenePharma | N/A |
| CircYAP ISH probe: GATTCTCTGGTTCATGGCTGTA TCCATCTCATCC(tttCATCATCATACATCATCAT) | Servicebio | N/A |
| circYAP pulldown negative control probe: TGGATGAGATGGATACAGCCATGAA | GenePharma | N/A |
| circYAP pulldown probe: TTCATGGCTGTATCCATCTCATCCA | GenePharma | N/A |
| **Recombinant DNA** | | |
| pcDNA3.1 | HANBIO | N/A |
| pcDNA3.1-circRNA1663 | HANBIO | N/A |
| psiCHECK2-PD-L1-NC | Ji Kai Gene Technology | N/A |

(*Continued on next page*)

*Continued*

| REAGENT or RESOURCE | SOURCE | IDENTIFIER |
|---|---|---|
| psiCHECK2-PD-L1-WT | Ji Kai Gene Technology | N/A |
| psiCHECK2-PD-L1-MUT | Ji Kai Gene Technology | N/A |
| Renilla-Luciferase plasmid | Ji Kai Gene Technology | N/A |
| pcDNA3.1 YAP1 | Ji Kai Gene Technology | N/A |
| pcDNA3.1 YAP1(Ser127 mut) | Ji Kai Gene Technology | N/A |
| pcDNA3.1 TCF4 | Ji Kai Gene Technology | N/A |
| Software and algorithms | | |
| GraphPad Prism 8 | GraphPad | N/A |
| SPSS 22.0 | IBM | N/A |
| Other | | |
| RPMI 1640 medium | Gibco | Cat# 11875119 |
| Dulbecco's Modified Eagle Medium | Gibco | Cat# 11995065 |
| fetal bovine serum | Clark Bioscience | Cat# FB15015 |

## RESOURCE AVAILABILITY

### Lead contact

Further information and requests for resources and reagents should be directed to and will be fulfilled by the lead contact, Dr. Zhenqiang Sun (fccsunzq@zzu.edu.cn).

### Materials availability

This study did not generate new unique reagents.

### Data and code availability

All data reported in this paper will be shared by the lead contact upon request.
This paper does not report original code.
Any additional information required to reanalyze the data reported in this paper is available from the lead contact upon request.

## EXPERIMENTAL MODEL AND SUBJECT DETAILS

### Clinical specimens

All clinical samples and follow-up data were collected from the First Affiliated Hospital of Zhengzhou University. Ethical approval was confirmed by the Ethics Committee of the First Affiliated Hospital of Zhengzhou University (2019-KY-423), and a written informed consent was signed by every patients.

### Cell lines

HCT116 cells, SW480 cells and Human embryonic kidney 293 T cells were obtained from the Shanghai Cell Bank of Chinese Academy of Sciences (Shanghai, China). HCT116 and SW480 cells were cultured in DMEM/high-glucose (Gibco, Carlsbad, CA, USA). Human embryonic kidney 293 T cells were cultured in RPMI 1640 (Gibco, Carlsbad, CA, USA). All cells were cultured supplemented with 10% fetal bovine serum (Clark Bioscience, Richmond, VA, USA) at 37 °Cand 5% CO2.

### Animals

All mouse procedures were approved by the Zhengzhou University Institutional Animal Care and Use Committee. Four-week-old female BALB/c nude mice purchased from Vital River Laboratory (Beijing, China). HuPBMC-NOG-dKO female mice purchased from Vital River Laboratory (Beijing, China).

### Statement of ethics

The present study was approved by the Ethics Committee of The First Afliated Hospital of Zhengzhou University (2019-KY-423).

## METHOD DETAILS

### Cell transfection of siRNAs and plasmids

siRNAs targeting circYAP1(siB171025053732 and siB171025053737), YAP1(siB160602113946), TCF4(siG1082132427), PD-L1(siG150520101800), YTHDF2(siG141112154420) and siRNA-NC (siN0000001-1-5) were designed and synthesized by RiboBio (Guangzhou, China). The circYAP1 overexpression plasmids and NC plasmids were purchased from Hanbio Biotechnology (Wuhan, China). The vector of YAP1 and TCF4 overexpression were constructed by Ji Kai Gene Technology Co.Ltd (Shanghai, China). Following strictly the manufacturer's instructions, siRNAs were transfected using Lipofectamine 3000 (Invitrogen, Thermo Fisher Scientific, Carlsbad, CA, USA), while plasmids using HieffTrans™ Liposome Transfection Reagent (Yeasen Biotechnology, Shanghai, China). Transfection efficiency detected by qRT-PCR.

### Total RNA isolation, reverse transcription and qRT-PCR

Total RNA was isolated from cells and tissues using RNAiso Plus (Takara, Dalian, China). After the concentration and purity of the total RNA were identified by NanoDrop 2000 (Termo Fisher Scientifc, Carlsbad, CA, USA), 1ug total RNA was reversed transcription to cDNA using uelris RT mix with DNase (All-in-One) (US Everbright® Inc, Suzhou, China). qRT- PCR was performed using the Hieff qPCR SYBR Green Master Mix kit (Yeasen, Shanghai, China) according to the manufacturer's instructions. All data were analyzed and normalized to GAPDH. All primers were shown in Table S1.

### RNase R treatment and actinomycin D assay

Total RNA of HCT116 and SW480 cells was digested with RNase R (5 U/μg RNA) (Lucigen, America) for 0min, 10min, 20min and 30 min at 37°C. Then, circYAP1 and YAP1 mRNA were detected by quantitative real-time PCR (qRT-PCR).

HCT116 and SW480 cells were cultured with 10ug/ml actinomycin D (Merck, Darmstadt, Germany) for 0h, 4h, 8h, 12h, and 20h. Total RNA from the cells was collected separately as planned. Then, circYAP1 and YAP1 mRNA were detected by qRT-PCR.

### RNA *in-situ* hybridization (ISH) and fluorescence *in-situ* hybridization (FISH)

For ISH, digoxin-labeled circYAP1 probe was synthesized by Servicebio (Wuhan, China). Tissue sections were dewaxed, prehybridized, and hybridized, and subsequently visualized using DAB. The H-score was determined by Servicebio (Wuhan, China).

For FISH, Cy3-circYAP1 probe was synthesized by GenePharma (Shanghai, China). HCT116 and SW480 cells were fixed for 30 min at room temperature. Then, according to the manufacturer's Instructions of FISH kit (RiboBio, Guangzhou, China) to complete the subsequent steps. Images were acquired by confocal laser scanning microscopy (Zeiss, Jena, Germany).

### Western blot analysis, immunofuorescence (IF), and immunohistochemistry (IHC)

Protein of HCT116 and SW480 cells was extracted with RIPA buffer containing protease inhibitors(P1005) and phosphatase inhibitors(P1081) and was quantified by a BCA kit (Beyotime, Shanghai, China). More details follow.[18] The following antibodies were used: anti-PD-L1 (Abcam, ab213524); anti-PD1(Abcam, ab137132); anti-IFN-γ(Abcam, ab231036) anti-CD8 alpha (Abcam, ab245118); anti-YAP (CST, No. 14074); anti-phospho-YAP (Ser127) (CST, No.13008); anti-TCF4 (Proteintech, No. 22337-1-AP); anti-YTHDF2 (CST, NO.71283); anti-Histone-H3 (Proteintech, No.17168-1-AP); anti-E-cadherin (Proteintech, No. 20874-1-AP); anti-N-cadherin (Servicebio, GB111009-100); anti-GAPDH (Proteintech, 60004–1-Ig). IF and IHC were performed according to manufacturer's instructions.

### CCK-8, EDU, migration and invasion assays

For CCK8, 48 hours after transfection, $2 \times 10^3$ CRC cells were seeded into 96-well culture plate. Cell Counting Kit-8 (Dojindo Laboratories, Kumamoto, Japan) was added at 0h, 24h, 48h and 72h, and the absorbance at 450nm was measured after 2 hours.

For EDU, 48 hours after transfection, $2 \times 10^4$ CRC cells were seeded into 96-well culture plate. After 24 hours, proliferation of CRC cells was determined by Cell-Light EdU Apollo567 *In Vitro* Kit (RiboBio, Guangzhou, China) according to the manufacturer's instructions.

For migration and invasion, 48 hours after transfection, $1 \times 10^5$ CRC cells seeded in upper chambers with 8-μm pore membranes (Corning, NY, USA) (without Matrigel for migration assay, with Matrigel for invasion assay). 600 μL DMEM medium with 20% FBS was added into bottom chambers. After 36 h, the migrated and invaded cells were fixed in 4% paraformaldehyde (Beyotime, Shanghai, China) and stained by crystal violet (Solarbio, Beijing, China), then photographed and counted using an optical microscope (Olympus, Tokyo, Japan).

### $CD8^+$ T cells isolation and incubation with CRC cells

Human $CD8^+$ T cells were acquired from healthy donors' peripheral blood by an Easy-Sep™ Direct Human $CD8^+$ T Cell Isolation Kit (STEMCELL Technologies). Human $CD8^+$ T cells were seeded into 24-well plates. Anti-CD3/anti-CD28 antibodies (STEMCELL Technologies) and Human Recombinant IL-2 were added to active $CD8^+$ T cells.

Modified CRC cells were seeded into 12-well plates. After 24 h, activated $CD8^+$ T cells were cocultured with CRC cells for 48 h at a ratio of 10:1.[44] After 48 h, $CD8^+$ T cells were collected to detect cytokine expression.

### RNA pull-down assay, RNA immunoprecipitation (RIP) and co-IP

Biotin-labeled circYAP1 probe and negative control probe were designed and synthesized by Genepharm (Shanghai, China). After 48 hours of transfection with the circYAP1 plasmid, CRC cells were collected for RNA pull-down assay according to the manufacturer's instructions of RNA pull-down kit (BersinBio, Guangzhou, China).

RIP assay was performed with YAP1 antibody, YTHDF2 antibody, anti-m6A antibody (Synaptic Systems, Goettingen, Germany) and anti-immunoglobulin G (IgG) (Millipore, MA, USA) using Magna RIP RNA-Binding Protein Immunoprecipitation Kit (Millipore, MA, USA) according to the manufacturer's instructions. Normalized to the input, the abundance of circYAP1 was assessed by qRT-PCR.

Co-IP assay was performed with anti-YAP1, anti-TCF4 and anti-IgG using Immunoprecipitation kit (Abcam, ab206996) according to the manufacturer's instructions. Interactions between YAP1 and TCF4 were assessed by western blot.

### Dual luciferase reporter assay

The sequence of wild type of PD-L1 promoter (PD-L1-wt), negative control (PD-L1-nc) and its mutant versions (PD-L1-mut) according to TCF4 protein binding sites were inserted into luciferase reporter vector psiCHECK2 (Ji Kai Gene Technology Co.Ltd, Shanghai, China). PD-L1-nc, PD-L1-wt and PD-L1-mut plasmids were co-transfected with TCF4 overexpression and NC plasmids into 293T cells. All groups were transfected with Renilla luciferase plasmids using HieffTrans™ Liposome Transfection Reagent (Yeasen Biotechnology, Shanghai, China). After 48h, luciferase activity was detected by the Dual-Luciferase Reporter Assay kit (Beyotime, Shanghai, China).

### Animal models

The lentiviral circYAP1 overexpression vector and NC were constructed using pHBLV-CMV-circ (Hanbio Biotechnology, Wuhan, China). According to the manufacturer's instructions, HCT116 cells after 72 hours of lentivirus infection were cultured using puromycin (2 μg/mL) to screen stable circYAP1-overexpression cell lines.

To observe the role of circYAP1 in regulating CRC metastasis *in vivo*, the stable cell lines of HCT116-LV-NC and HCT116-LV-CircYAP1 ($2\times10^6$ in 100 μL of PBS) were injected into the tail vein of four-week-old female BALB/c nude mice purchased from Vital River Laboratory (Beijing, China). On day 42, mice were sacrifced and lungs were collected for HE staining and IHC.

To observe the role of circYAP1 in regulating CRC proliferation and immune evasion *in vivo*, HCT116-LV-NC and HCT116-LV-CircYAP1($6\times10^6$ in 100 μL of PBS) were inoculated into subcutaneous dorsal flanks of huPBMC-NOG-dKO female mice purchased from Vital River Laboratory (Beijing, China). On day 33, mice were sacrificed and tumor were collected for HE staining and IHC.

All mouse procedures were approved by the Zhengzhou University Institutional Animal Care and Use Committee.

## QUANTIFICATION AND STATISTICAL ANALYSIS

All data were analyzed using GraphPad Prism 8.0 (GraphPad, San Diego, CA, USA) and shown as mean ± standard deviation (SD). Continuous data differences analysis was evaluated by Student's t-test between two groups. One-way analysis of variance (ANOVA) test was used to analyze differences among multiple groups. Survival curves were assessed using Kaplan-Meier's method and log-rank tests. Correlations were assessed by Spearman correlation coefficient analyses. $P<0.05$ was considered significant. ns $P>= 0.05$, *$P < 0.05$, **$P < 0.01$, ***$P < 0.001$, ****$P < 0.0001$. Statistical details for each experiment are included in the figures and figure legends.